

# MetaWave: A Platform for Unified Implementation of Nonrelativistic and Relativistic Wavefunctions

Ning Zhang, Qingpeng Wang, and Wenjian Liu\*

*Qingdao Institute for Theoretical and Computational Sciences and Center for Optics Research  
and Engineering, Shandong University, Qingdao 266237, China*

E-mail: liuwj@sdu.edu.cn

## Abstract

MetaWave is a C++ template-based architecture designed for unified implementation of nonrelativistic and relativistic wavefunction-based quantum chemical methods. It is highly modular, extendable, and efficient. This is achieved by decoupling the three distinct aspects of quantum chemical methods (i.e., nature of Hamiltonian, structure of wavefunction, and strategy of parallelization), thereby allowing for separate treatment of them through their internal type-trait and tagging systems furnished by C++ metaprogramming. Once the second-quantized Hamiltonians, whether non-relativistic (spin-free) or relativistic (spin-dependent), are decomposed into topologically equivalent diagrams for a unified evaluation of the basic coupling coefficients between (randomly selected) spin-free or spin-dependent configuration state functions or Slater determinants incorporating full molecular symmetry (including single or double point group and spin or time reversal symmetry), the many-electron wavefunctions, whether built up with scalar or spinor orbitals, can be assembled with the same templates. As for parallelization, MetaWave supports both OpenMP and MPI,

with the majority of the latter being translated automatically from its OpenMP counterparts. The whole structure of MetaWave is reviewed here, with some showcases for illustrating its performance.

# 1 Introduction

As emphasized recently,<sup>1</sup> high-precision spectroscopic calculations ought to treat relativistic, correlation, and quantum electrodynamics (QED) effects on an equal footing, so as to match experimental measurements as closely as possible. Since both relativistic and QED effects can be incorporated into second-quantized Hamiltonians,<sup>2-5</sup> which take the same form as the nonrelativistic (spin-free) one, it would be nice if all second-quantized Hamiltonians can be manipulated in the same way for subsequent development of wavefunction methods for describing electron correlation. This is indeed possible, thanks to two recent developments: (1) relativistic-QED Hamiltonians, whether four-component or two-component, can be constructed in a unified manner based solely on physical arguments;<sup>6</sup> (2) all second-quantized Hamiltonians can be decomposed into topologically equivalent diagrams, such that the basic coupling coefficients between (randomly selected) spin-free or spin-dependent configuration state functions (CSF) or Slater determinants (DET) can be evaluated in a unified manner.<sup>7</sup> What is left is then how to design and implement many-electron wavefunctions for describing electron correlation as accurately as possible. The so-called strongly correlated systems of electrons, such as extended  $\pi$  systems and polynuclear transition metal clusters, are particularly intricate in this aspect, due to the fact that the static and dynamic components of the overall correlation are therein strongly entangled and even interchangeable. The currently best methods for such kinds of systems include density matrix renormalization group (DMRG)<sup>8-14</sup> and selected configuration interaction (sCI) plus second-order perturbation theory (sCIPT2).<sup>7,15-39</sup>

Given so many wavefunction methods, the question is how to extend them to the relativistic realm, yet without significant code rewriting. To address this, we first outline the general aspects of wavefunctions methods:

## 1. Nature of Hamiltonian

To implement a wavefunction method, the very first thing under concern is the

nature of the chosen Hamiltonian, spin-free or spin-dependent. While molecular orbitals can be chosen to be real-valued in the spin-free case, they are necessarily complex-valued in the spin-dependent case. This leads to different permutation and point group symmetries to molecular integrals and hence different data structure for their storage.

## 2. Structure of Wavefunction

$N$ -electron wavefunctions can be expanded in terms of Hilbert space basis states (HSS) or Fock space basis states (FSS). Every member of the former carries  $N$ -electrons and  $N$  spin orbitals, whereas that of the latter may have a variable number of electrons and even a variable number of spin orbitals. For instance, the well-established many-body perturbation theory (MBPT), coupled-cluster (CC), and configuration interaction (CI) types of wavefunctions are all built up with an  $N$ -electron mean-field (Hartree-Fock or CASSCF) reference and additional  $N$ -electron configurations generated from it by systematic excitations/replacements. No matter how such HSSs are herein truncated, antisymmetry is always maintained automatically. In contrast, when working with *local* FSSs as in DMRG wavefunctions, suitable constraints must be imposed from the outside to conserve the number ( $N$ ) of electrons and antisymmetry. In essence, the two kinds of representations access electron correlation through different routes: the HSS representation tries to improve the initial independent-particle description by selecting low-energy  $N$ -electron functions from the (first-order) interacting Hilbert space, ending up with a linear (in CI) or nonlinear (in CC) combination of limited HSS, whereas the local FSS representation attempts to improve the initial independent-subsystem description by selecting high-entanglement local states from the renormalized Fock space, ending up with a particular linear combination of *all* HSS. The symmetry adaptation of HSS can be achieved by using appropriate irreducible representations (irrep) of the  $U(n)$  and single point groups in the spin-free case, whereas by using time reversal and dou-

ble point groups in the spin-dependent case. In contrast, the symmetry adaptation of local FSS has to be performed in terms of local symmetry operations in both the spin-free<sup>40,41</sup> and spin-dependent<sup>42</sup> cases. Additionally, the implementation has to distinguish between complex and real algebras associated with spin-dependent and spin-free wavefunctions, respectively.

### 3. Strategy of Parallelization

The efficient execution of wavefunction methods relies on proper parallelization and hardware-specific optimizations. Different parallelization patterns (e.g., OpenMP or MPI) or hardware platforms (e.g., CPU, GPU or their hybrid<sup>43,44</sup>) typically necessitates substantial code rewrites.

To achieve a unified implementation of wavefunction methods, the above aspects must be decoupled as much as possible. To this end, we design here a platform, *MetaWave*, which can treat the three aspects separately through their internal type-trait<sup>1</sup> and tagging<sup>2</sup> systems furnished by C++ metaprogramming. What is essential is the use of a template to generate temporary subroutines, which are then merged with other relevant codes and compiled. This strategy reduces significantly code duplication and enhances maintainability as the software expands. Use of *MetaWave* has been made to achieve a unified implementation<sup>7</sup> of the nonrelativistic<sup>16,17</sup> and relativistic<sup>7,36</sup> variants of the fully symmetry adapted iCIPT2 (iterative configuration interaction with selection and second-order perturbation) method. Note in passing that the idea of decoupling different aspects of wavefunction methods was already adopted in the HORTON program package,<sup>45</sup> where the Fanpy library<sup>46</sup> is also highly modular and general for implementing new wavefunction methods based on the flexible ansätze for  $N$ -electron configuration interaction (FANCI)<sup>47</sup>

---

<sup>1</sup>Type traits are compile-time tools in C++ that provide information about types (e.g., inquiry whether a type represents the nonrelativistic Hamiltonian). This enables functions or templates to automatically adjust their behavior based on the types they handle, enhancing flexibility and type safety.

<sup>2</sup>A tag in C++ is an empty struct to label concepts. For example, one can use a struct `NonRelativistic` to label nonrelativistic Hamiltonian. Combined with type-traits, this will enable compilers to process information related to the nonrelativistic Hamiltonian.

and perturbation theory (FANPT) frameworks.<sup>48</sup> However, Fanpy is a research tool written purely in Python, with the primary goal being quick implementation and test of a new wavefunction ansatz, instead of high-performance parallel computing. Moreover, Fanpy does not support relativistic Hamiltonians and wavefunctions, which are the primary concern of MetaWave.

The remaining of the paper is organized as follows. Sec. 2 is devoted to general features of the sCIPT2 methods, including unified treatments of Hamiltonians, many-particle basis functions (MPBF), and Hamiltonian matrix elements (HME), selection procedures, and proper implementation of the Epstein-Nesbet second-order perturbation theory (ENPT2).<sup>49,50</sup> The three-layer architecture of MetaWave is then presented in detail in Sec. 3. As a showcase, the computational costs of sf-X2C-iCIPT2, SOiCI, and 4C-iCIPT2 are briefly compared in Sec. 4. The paper is finally closed with concluding remarks in Sec. 5.

## 2 sCIPT2

The available nonrelativistic<sup>15–25,27–35</sup> and relativistic<sup>7,36–39</sup> sCIPT2 methods implemented in several program packages<sup>51–56</sup> all involve three major steps, i.e., preparation of a guess space  $P_0$ , iterative update of the variational space until convergence, and second-order perturbation correction to the energy. However, they differ in the actual implementations, which involve the following issues (see Fig. 1):

1. How to assess and rank the importance of the CSFs/DETs outside of the variational space  $P_0$ , so as to expand  $P_0$  to  $P_1$ ?
2. How to diagonalize  $P_1$  in the pruning step, so as to reduce  $P_1$  to  $P_2$ ?
3. How to terminate the selection process?
4. How to estimate the contribution of the discarded CSFs/DETs?

Herewith, we introduce a general algorithm that is suitable for different Hamiltonians, MPBFs, and parallelization schemes.

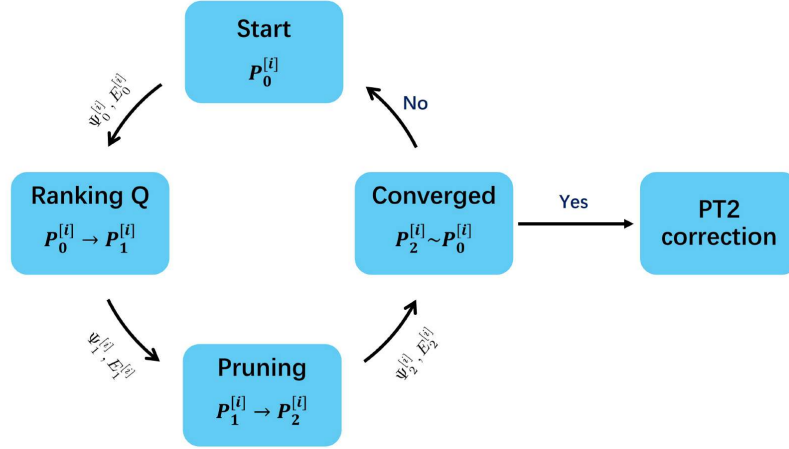


Figure 1: Workflow of sCIPT2

## 2.1 Unified Handling of Hamiltonians

All Hamiltonians in ab initio quantum chemistry, whether spin-free or spin-dependent, take the following generic, second-quantized form

$$H = \sum_{ij} h_{ij} E_{ij} + \frac{1}{2} \sum_{i,j,k,l} (ij|kl) e_{ij,kl} = H^\dagger \quad (1)$$

$$E_{ij} = a_i^\dagger a_j = E_{ji}^\dagger \quad (2)$$

$$e_{ij,kl} = a_i^\dagger a_k^\dagger a_l a_j = e_{kl,ij} = e_{ji,lk}^\dagger = e_{lk,ji}^\dagger \quad (3)$$

Here,  $\{i, j, k, l\}$  refer to molecular orbitals/spinors obtained by a mean-field calculation, whereas  $h_{ij}$  and  $(ij|kl)$  (in the Mulliken notation) are the integrals of the core Hamiltonian and two-body operators, respectively. It should be emphasized that, in the spin-dependent case, the molecular spinors are assumed here to be symmetrized<sup>57</sup> according

to both double point group and time reversal symmetries, such that they can be grouped into  $n$  Kramers pairs  $\{\psi_i, \psi_{\bar{i}} = \mathcal{K}\psi_i\}_{i=1}^n$ , where  $\mathcal{K}$  ( $= -i\mathbf{I}_2 \otimes \sigma_y K_0$ ) is the time reversal operator (NB:  $K_0$  represents complex conjugation). By making only use of the permutation symmetry of the molecular integrals, Eq. (1) can be decomposed as<sup>16</sup>

$$H = H_1^0 + H_2^0 + H_1^1 + H_2^1 + H_2^2 \quad (4)$$

$$H_1^0 = \sum_i h_{ii} E_{ii} \quad (5)$$

$$H_1^1 = \sum_{i<j} h_{ij} E_{ij} + \sum_{i>j} h_{ij} E_{ij} \quad (6)$$

$$H_2^0 = \frac{1}{2} \sum_i (ii|ii) E_{ii} (E_{ii} - 1) + \sum_{i<j} [(ii|jj) E_{ii} E_{jj} + (ij|jj) e_{ij,ji}] \quad (7)$$

$$H_2^1 = \sum_{i \neq j} [(ii|ij) (E_{ii} - 1) E_{ij} + (ij|jj) E_{ij} (E_{jj} - 1)] + \sum_{i \neq j \neq k} [(ij|kk) E_{ij} E_{kk} + (ik|kj) e_{ik,kj}] \quad (8)$$

$$H_2^2 = \sum_{i \leq k} \sum'_{j \leq l} \left[ 2^{-\delta_{ik} \delta_{jl}} (ij|kl) e_{ij,kl} + (1 - \delta_{ik}) (1 - \delta_{jl}) (il|kj) e_{il,kj} \right] \quad (9)$$

where the superscripts of  $H_i$  ( $i = 1, 2$ ) classify the excitation levels (zero, single or double) between a pair of orbital configurations (oCFG), whereas the prime in the summation of  $H_2^2$  indicates that  $\{j, l\} \cap \{i, k\} = \emptyset$ . The individual terms of  $H_i^j$  ( $i = 1, 2; j = 0, 1, 2$ ) can be represented pictorially by the diagrams shown in Figs. 2 to 4, which are drawn with the following conventions: (1) The enumeration of orbital/spinor levels starts with zero and increases from bottom to top. (2) The left and right vertices (represented by filled diamonds) indicate creation and annihilation operators, respectively, which form a single generator when connected by a non-vertical line. (3) Products of single generators should always be understood as normal ordered. For instance, Fig. 3(m) means  $\{E_{ik} E_{kj}\} = \{E_{kj} E_{ik}\} = E_{ik} E_{kj} - E_{ij} = e_{ik,kj}$  ( $i < j < k$ ), which is the exchange counterpart of the

direct generator  $\{E_{ij}E_{kk}\} = \{E_{kk}E_{ij}\} = e_{ij,kk}$  ( $i < j < k$ ) shown in Fig. 3(g). The same diagrams can be used to compute the basic coupling coefficients (BCC) between spin-free<sup>58</sup> or between spin-dependent<sup>7</sup> CSFs/DETs. It is just that, in the spin-dependent case, every vertex of the diagrams [i.e., every term in the algebraic expressions (5) to (9)] is composed of both unbarred (A) and barred (B) spinors (e.g., the first term of  $H_2^0$  (7) is composed of 16 terms, in stead of merely one term as in the spin-free case). As a matter of fact, due to the underlying hermiticity, only the  $s_2$ ,  $c_x$  ( $x \in [1,6]$ ), and  $d_x$  ( $x \in [1,7]$ ) types of diagrams are needed for computing the one- and two-particle BCCs. That is, once the BCCs for these types of diagrams are available, those for the conjugate diagrams can be obtained simply by matrix conjugate transpose. In particular, the tabulated unitary group approach (TUGA)<sup>16,17</sup> can be employed to evaluate and reuse the BCCs between randomly selected spin-free or spin-dependent CSFs/DETs. The decomposed form (4) of the Hamiltonian (1) offers an additional advantage: by using oCFGs as the organization unit, the same set of integrals can be utilized for multiple HMEs (vide post). In particular, some upper bounds  $\tilde{H}^{IJ}$  for the HMEs between the CSFs/DETs of oCFG pairs  $|I\rangle$  and  $|J\rangle$  can be established<sup>17</sup> in advance (cf. Table 1) and then used to facilitate the selection procedure.

It deserves to be mentioned that the above diagrammatic representation of the Hamiltonians can also be used in DMRG working with matrix product states/operators (MPS/MPO). To see this, recall first that the spin-free BCC  $\langle I\mu|E_{ij}|J\nu\rangle$  is evaluated in UGA<sup>58</sup> via product of the segment values  $W_r$ ,

$$\langle I\mu|E_{ij}|J\nu\rangle = \prod_{r=1}^n W(Q_r; \tilde{d}_r d_r, \Delta b_r, b_r) =: \prod_{r=1}^n W_r \quad (10)$$

where  $\{d_r\}_{r=1}^n$  are the Shavitt step numbers<sup>59</sup> [NB:  $b_r$  can be derived from  $d_p$  ( $p \in [1, r]$ ) and  $\Delta b_r = b_r - \tilde{b}_r$ ], in terms of which the bar and ket CSFs can be expressed as  $|I\mu\rangle = |\tilde{d}_1 \cdots \tilde{d}_n\rangle$  and  $|J\nu\rangle = |d_1 \cdots d_n\rangle$ , respectively. In contrast, in the MPO/MPS formalism<sup>60</sup>

of DMRG, the Hamiltonian and wavefunctions are expressed as

$$H = \sum_{\{\sigma_k, \sigma'_k\}} \left( \sum_{\{\beta_k\}} O_{\beta_1}^{\sigma_1 \sigma'_1} [1] O_{\beta_1, \beta_2}^{\sigma_2 \sigma'_2} [2] \cdots O_{\beta_{n-1}}^{\sigma_n \sigma'_n} [n] \right) |\sigma_1 \sigma_2 \cdots \sigma_n\rangle \langle \sigma'_1 \sigma'_2 \cdots \sigma'_n| \quad (11)$$

$$|\tilde{\Psi}\rangle = \sum_{\{\sigma_k\}} \left( \sum_{\{\alpha_k\}} \tilde{A}_{\alpha_1}^{\sigma_1} [1] \tilde{A}_{\alpha_1 \alpha_2}^{\sigma_2} [2] \cdots \tilde{A}_{\alpha_{n-1}}^{\sigma_n} [n] \right) |\sigma_1 \sigma_2 \cdots \sigma_n\rangle \quad (12)$$

$$|\Psi\rangle = \sum_{\{\sigma_k\}} \left( \sum_{\{\alpha_k\}} A_{\alpha_1}^{\sigma_1} [1] A_{\alpha_1 \alpha_2}^{\sigma_2} [2] \cdots A_{\alpha_{n-1}}^{\sigma_n} [n] \right) |\sigma_1 \sigma_2 \cdots \sigma_n\rangle \quad (13)$$

Here,  $\{\sigma_k\}$  are physical bonds, whereas  $\{\alpha_k\}$  and  $\{\beta_k\}$  are virtual bonds. The transition matrix element  $\langle \tilde{\Psi} | H | \Psi \rangle$  can then be calculated as

$$\langle \tilde{\Psi} | H | \Psi \rangle = \mathbf{E}[1] \mathbf{E}[2] \cdots \mathbf{E}[n] \quad (14)$$

where the transfer matrices are defined as

$$E[i]_{\alpha_{i-1} \beta_{i-1} \alpha'_{i-1} \alpha_i \beta_i \alpha'_i} = \sum_{\sigma_i, \sigma'_i} \tilde{A}_{\alpha_{i-1} \alpha_i}^{\sigma_i} O_{\beta_{i-1} \beta_i}^{\sigma_i \sigma'_i} A_{\alpha'_{i-1} \alpha'_i}^{\sigma'_i} \quad (15)$$

It follows that Eq. (14) is an analog of Eq. (10) (see Fig. 5 for their graphical representations). For instance, if both  $\tilde{\Psi}$  and  $\Psi$  are single DETs and  $H = E_{ij}$ , then  $\mathbf{E}(i)$  (with all bond dimensions equal to one) plays the same role as the segment value  $W_i$  in Eq. (10). In general, the MPO representation (11) of a full Hamiltonian  $H$  involves splittings of the diagrams in Figs. 2 to 4 into products of partial diagrams, each of which represents a local operator (i.e.,  $O_{\beta_{i-1} \beta_i}^{\sigma_i \sigma'_i}$  with specific values for the four bonds). The direct sum of such local operators for all relevant diagrams then gives rise to the tensor operator  $O[i]$ .

In short, the present diagrammatic representation of the spin-free/dependent Hamiltonians (which can be extended to include multicomponent Hamiltonians<sup>61,62</sup> and those involving electron-phonon coupling and matter-light interactions<sup>63–65</sup>) unifies the eval-

uation of matrix elements via Slater-Condon rules, UGA, and MPO/MPS. Nevertheless, the formulation of spin-adapted MPOs/MPSs in terms of the Shavitt graphs<sup>59</sup> remains to be further investigated. Moreover, it should be mentioned that some tensor contraction engine should further be incorporated into MetaWave for unified implementation of relativistic and nonrelativistic CC methods.

Table 1: Correspondence between UGA Diagrams<sup>58</sup> (see Figs. 2 to 4) and integral categories (IntC) as well as Upper Bounds  $\tilde{H}^{IJ}$  for Hamiltonian Matrix Elements over CSFs/DETs

IntC	operator	range	diagram	$\tilde{H}^{IJ}$	
				CSF	SD
0	$E_{ij}$	$i > j$	s2		
		$i > j > k$	c4		
	$e_{ik,kj}$	$k > i > j$	c6		
		$i > k > j$	d2		
1	$e_{ij,kl}$	$k > l > j > i$	c1		
	$e_{il,kj}$		c3		
2	$e_{ij,kl}$	$k > l > i > j$	d1	$\max( (ij kl) + (il kj) , \sqrt{3} (ij kl) - (il kj) )$	$\max( (ij kl) ,  (il kj) )$
	$e_{il,kj}$		c5		
3	$e_{ij,kl}$	$k > i > l > j$	d3		
	$e_{il,kj}$		d5		
4	$e_{ij,kj}$	$k > j > i$	c2		
5	$e_{ij,kj}$	$k > i > j$	d4	$2 (ij kj) $	$ (ij kj) $
6	$e_{il,ij}$	$i > l > j$	d6	$2 (il ij) $	$ (il ij) $
7	$e_{ij,ij}$	$i > j$	d7	$ (ij ij) $	$ (ij ij) $

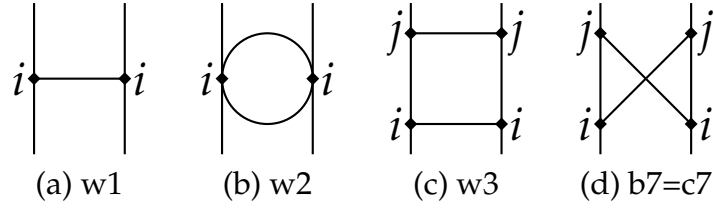


Figure 2: Diagrammatic representation of  $H_1^0$  (a) and  $H_2^0$  (b-d). The naming of the diagrams follows Ref. 58

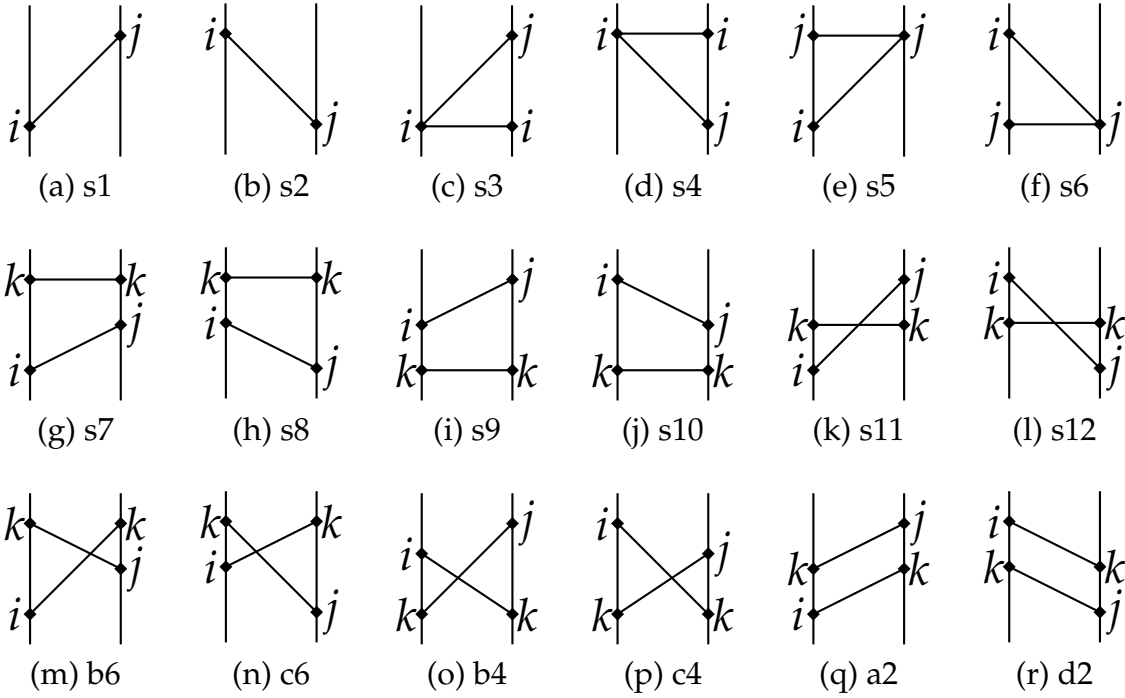


Figure 3: Diagrammatic representation of  $H_1^1$  (a-b) and  $H_2^1$  (c-r). The naming of the diagrams follows Ref. 58

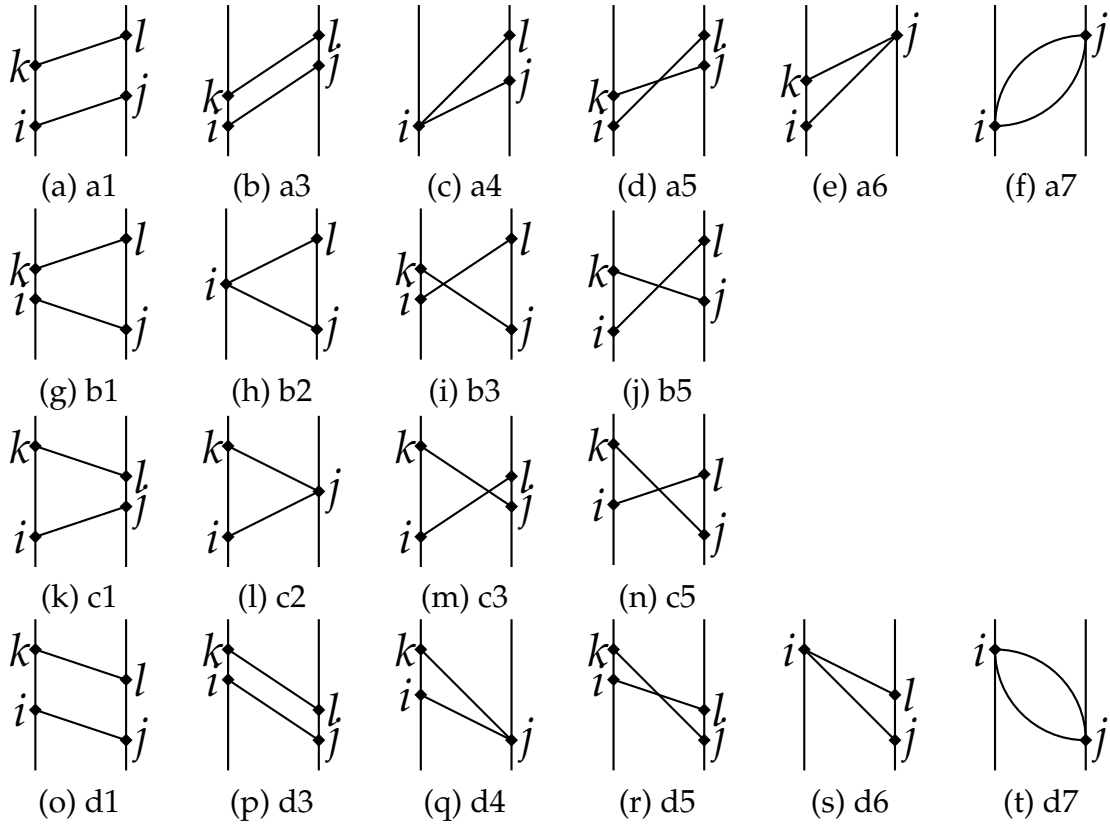


Figure 4: Diagrammatic representation of  $H_2^2$ . The naming of the diagrams follows Ref. 58

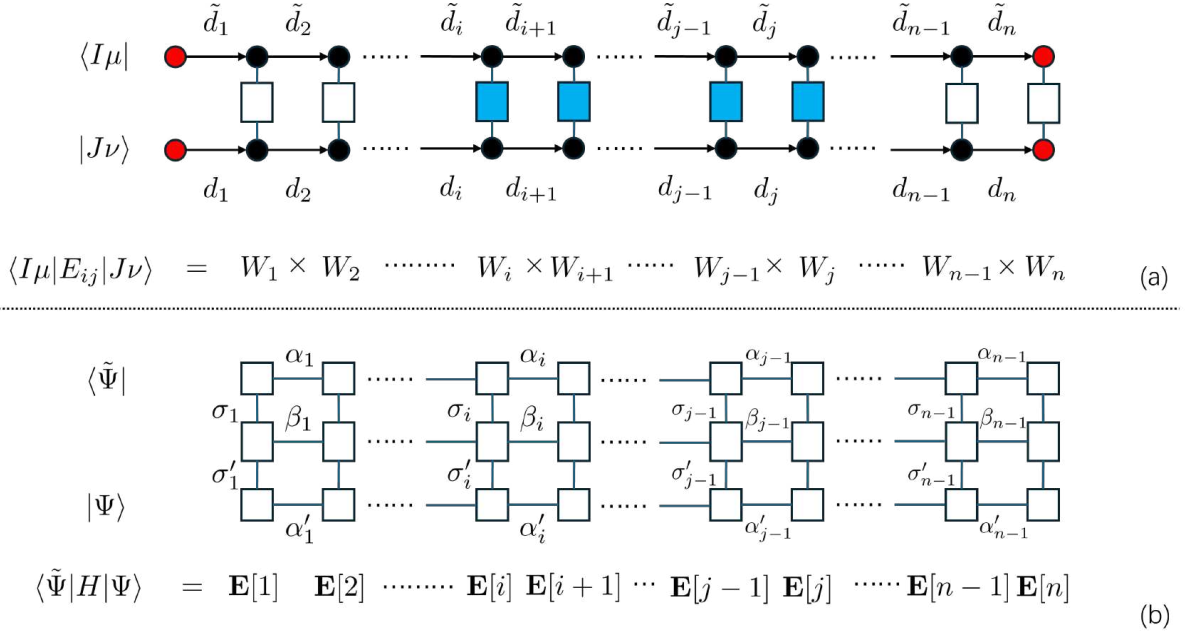


Figure 5: Graphical representations of (a) product of segment values  $W_r$  ( $r \in [1, n]$ ) in Eq. (10) and (b) product of transfer matrices  $\mathbf{E}(i)$  ( $i \in [1, n]$ ) in Eq. (14).

## 2.2 Unified Handling of MPBFs

To achieve a unified handling of MPBFs, the oCFGs are taken as the organization unit in MetaWave. An oCFG  $|I\rangle$ , defined by a set of occupation numbers  $\in \{0, 1, 2\}$  for the  $n$  spatial orbitals in the spin-free case or  $n$  Kramers pairs of spinors in the spin-dependent case, can be represented by a binary string composed of an array of 64-bit unsigned integers (2 bits for each spatial orbit/Kramers pair), viz.

$$\underbrace{(n_{31}^1 \cdots n_0^1, \dots, n_{31}^k \cdots n_0^k)}_{\text{array of 64-bit integers}} = \underbrace{|n_0^1 \cdots n_{31}^1 \cdots n_0^k \cdots n_{31}^k\rangle}_{\text{orbital configuration}} \quad (16)$$

where  $n_p^q = 0, 1, 2$  are represented by  $(00)_2$ ,  $(01)_2$ , and  $(11)_2$ , respectively. Here, the number of bit 1 coincides with the occupation number, thereby enabling efficient bitwise operations on oCFGs.<sup>16,17</sup> An oCFG  $|I\rangle$  can generate a number of CSFs/DETs denoted as  $|I\mu\rangle$ , where  $\mu$  distinguishes different spin-coupling schemes for CSFs or distributions of open-shell spins/Kramers partners for DETs.

### 2.3 Unified Construction of Hamiltonian Matrix

The HMEs  $\langle I\mu|H|J\nu\rangle$  involve contractions between the integrals and BCCs, the reuse of which must be maximized in sCI methods due to the lack of structures (natural connections). To facilitate this, we classify the HMEs into three ‘matrix element categories’ (MEC) corresponding to zero-, single-, and two-electron differences between oCFGs  $|I\rangle$  and  $|J\rangle$ , and meanwhile classify the two-electron integrals into seven ‘integral categories’ (IntC  $\in [1, 7]$  in Table 1). Each MEC/IntC involves only a subset of the integrals determined by the oCFG pair  $(I, J)$  rather than by the individual MPBFs. For the cases with zero- and one-electron differences, the HMEs can be simplified by introducing a closed-shell reference oCFG  $|\omega\rangle$  in both the spin-free<sup>16</sup> and spin-dependent<sup>7</sup> cases.

As for the reuse of the BCCs, a key observation lies in that doubly occupied or unoccupied orbitals common to the oCFG pair  $(I, J)$  can be permuted freely with other orbitals without changing the BCCs, provided that the Yamaguchi–Kotani phase is employed in the case of CSFs.<sup>58</sup> Consequently, they can be deleted, leading to a reduced oCFG pair  $(\tilde{I}, \tilde{J})$  spanned by the reduced set of orbitals  $\tilde{r} \in [\tilde{1}, \tilde{N}]$ , with  $\tilde{N}$  being the number of common singly occupied orbitals and those orbitals with different occupations in  $|\tilde{I}\rangle$  and  $|\tilde{J}\rangle$ . In this way, the BCCs  $\langle I\mu|E_{ij}|J\nu\rangle$  and  $\langle I\mu|e_{ij,kl}|J\nu\rangle$  can simply be calculated as  $\langle \tilde{I}\mu|E_{\tilde{i}\tilde{j}}|\tilde{J}\nu\rangle$  and  $\langle \tilde{I}\mu|e_{\tilde{i}\tilde{j},\tilde{k}\tilde{l}}|\tilde{J}\nu\rangle$ , respectively. The orbital sequence and occupation pattern of  $(\tilde{I}, \tilde{J})$  can be encoded into a reduced occupation table (ROT)<sup>16</sup> as the internal representation in MetaWave. Different oCFG pairs but of the same ROT share the same BCCs. Moreover, due to Hermiticity of the BCCs, only those ROTs with  $\tilde{I} \geq \tilde{J}$  are needed in practical appli-

cations, thereby achieving optimal reuse of the BCCs.

The general scheme for evaluating bunches of HMEs is as follows:

1. Classify the given set of oCFG pairs  $\{(I, J)\}$  according to the MECs and then establish the ROTs for each MEC;
2. Sort oCFG pairs  $\{(I, J)\}$  according to the ROTs;
3. Fetch the integrals according to the IntCs;
4. Evaluate the BCCs on the fly across all oCFG pairs sharing the same ROT, and then contract with different integrals for different HMEs.

In summary, different Hamiltonians, different MPBFs, and unstructured HMEs can be treated in unified manners within MetaWave.

## 2.4 Selection

The aim of selection is to find iteratively an improved variational space for the expansion of the wavefunction. It involves four key components, i.e., ranking, diagonalization (of  $P_1^{[i]}$  in Fig. 1), pruning, and termination. To simplify the notation, the variational space and its first-order interacting space (FOIS) are denoted here as  $P$  and  $Q$ , respectively. The former gives rise to the target states  $\{E_k^{(0)}, |\Psi_k^{(0)}\rangle = \sum_{J\nu \in P} |J\nu\rangle C_{\nu,k}^J\}$ .

In view of MBPT, the most rigorous ranking criterion for the importance of a CSF or DET  $|I\mu\rangle \in Q$  is the absolute value of its first-order coefficient

$$f(|I\mu\rangle) = \max_k \left| \frac{\sum_{|J\nu\rangle \in P} H_{\mu\nu}^{IJ} C_{\nu,k}^J}{E_k^{(0)} - H_{\mu\mu}^{II}} \right|, \quad H_{\mu\nu}^{IJ} = \langle I\mu | H | J\nu \rangle \quad (17)$$

or similarly the absolute value of its second-order energy correction to the variational energy  $E_0$

$$\epsilon(|I\mu\rangle) = \max_k \left| \frac{|\sum_{|J\nu\rangle \in P} H_{\mu\nu}^{IJ} C_{\nu,k}^J|^2}{E_k^{(0)} - H_{\mu\mu}^{II}} \right| \quad (18)$$

Note in passing that the perturbative estimate (18) of  $\epsilon(|I\mu\rangle)$  can also be replaced<sup>66</sup> with that obtained by diagonalizing the Hamiltonian over the two-state system  $\{\Psi_0, |I\mu\rangle\}$ . Such ‘CIPSI criterion’ can be used in different ways when constructing the  $P$  space iteratively. For instance, all  $\{|I\mu\rangle\} \in Q$  with  $f(|I\mu\rangle)$  larger than a preset threshold  $C_Q$  are retained in the variational space  $P$  at each iteration of CIPSI (configuration interaction with perturbative selection made iteratively).<sup>67</sup> It is obvious that the final size of  $P$  (denoted as  $|P|$ ) is determined by the threshold  $C_Q$  itself. A variant<sup>68</sup> of CIPSI is that those  $\{|I\mu\rangle\} \in Q$  with the largest  $\epsilon(|I\mu\rangle)$  are put into  $P$  until the target size  $|P|$  has reached. An additional constraint is invoked in ASCI (adaptive sampling configuration interaction),<sup>30</sup> where except for  $|P|$ ,  $|Q|$  is also kept fixed throughout the iterative selections, by making use of  $f(|I\mu\rangle)$ . A different strategy is adopted in ACI (adaptive configuration interaction),<sup>27</sup> where those  $\{|I\mu\rangle\} \in Q$  of the smallest  $\epsilon(|I\mu\rangle)$  are excluded as long as the sum of their  $\epsilon(|I\mu\rangle)$  is smaller than the target accuracy of energy. At variance with these implementations which feature two spaces ( $P$  and  $Q$ ), ICE (iterative configuration expansion)<sup>35</sup> adopts the three-space concept,<sup>69</sup> where the  $P$  space is split into two subspaces spanned by the generators and the rest (spectators), which have weights larger and smaller than a threshold, respectively. Only the former are allowed to access perturbers  $\{|I\mu\rangle\} \in Q$ , which are included in the  $P$  space only when their  $\epsilon(|I\mu\rangle)$  are larger than a second threshold.

Noticing that the CIPSI criterion (17)/(18) is computationally too expensive (due to the summation in the numerator), a drastically simplified criterion was introduced in SHCI (semi-stochastic heat-bath configuration interaction),<sup>19</sup> viz.

$$f(|I\mu\rangle, |J\rangle, \eta_Q) = \max_{v,k} \left| H_{\mu\nu}^{IJ} C_{v,k}^J \right| \geq \eta_Q \quad (19)$$

It follows that those  $|I\mu\rangle \in Q$  with  $|H_{\mu\nu}^{IJ}| < \eta_Q / \max_k |C_{v,k}^J|$  are never touched (cf. Fig. 6), provided that the integrals are pre-sorted in descending order of their magnitudes.

However, such integral-driven selection usually leads to a variational space  $P$  that is much less compact<sup>17</sup> than that by using the coefficient/energy-driven selection (17)/(18). To remedy this but retaining the efficiency, the good of the integral- and coefficient-driven selections is combined in iCIPT2,<sup>16,17</sup> by means of the following boolean function  $f(|I\mu\rangle, |J\rangle, C_{\min})$ :

(A) If  $|I\rangle$  is identical with or singly excited from  $|J\rangle \in P$ , then

$$f(|I\mu\rangle, |J\rangle, C_{\min}) = \left( \max_{v,k} \left( |H_{\mu\nu}^{IJ} C_{v,k}^J| \right) \geq C_{\min} \right) \quad \text{and} \\ \left( \max_{v,k} \left( \left| \frac{H_{\mu\nu}^{IJ} C_{v,k}^J}{E_k^{(0)} - H_{\mu\mu}^{II}} \right| \right) \geq C_{\min} \right) \quad (20)$$

(B) If  $|I\rangle$  is doubly excited from  $|J\rangle \in P$ , then

$$f(|I\mu\rangle, |J\rangle, C_{\min}) = \left( \max_{v,k} \left( |\tilde{H}^{IJ} C_{v,k}^J| \right) \geq C_{\min} \right) \quad \text{and} \\ \left( \max_{v,k} \left( |H_{\mu\nu}^{IJ} C_{v,k}^J| \right) \geq C_{\min} \right) \quad \text{and} \quad (21) \\ \left( \max_{v,k} \left( \left| \frac{H_{\mu\nu}^{IJ} C_{v,k}^J}{E_k^{(0)} - H_{\mu\mu}^{II}} \right| \right) \geq C_{\min} \right)$$

Literally, for case (A), loop over  $|I\mu\rangle$  in  $Q$  and evaluate  $H_{\mu\nu}^{IJ}$  for all CSFs  $|J\nu\rangle \in P$ . If  $\max_{v,k} \left( |H_{\mu\nu}^{IJ} C_{v,k}^J| \right)$  is larger than  $C_{\min}$  then evaluate  $H_{\mu\mu}^{II}$ ; otherwise discard  $|I\mu\rangle$ . If  $\max_{v,k} \left( \left| \frac{H_{\mu\nu}^{IJ} C_{v,k}^J}{E_k^{(0)} - H_{\mu\mu}^{II}} \right| \right)$  is larger than  $C_{\min}$  then  $|I\mu\rangle$  is selected. As for case (B), only those doubly excited oCFGs  $|I\rangle$  with estimated upper bounds  $\tilde{H}^{IJ}$  (cf. Table 1) larger than  $C_{\min} / \max_{v,k} |C_{v,k}^J|$  need to be generated (i.e., those unimportant ones are never touched, see Fig. 6). For such  $\{|I\rangle\}$ , the remaining step is the same as case (A).

It should be noted that not all CSFs/DETs have appreciable weights in the wavefunction ( $\Psi_1^{[i]}$  in Fig. 1), even with the above ranking. Therefore, those CSF/DETs of very small coefficients should be deleted to end up with a compact varitional space ( $P_2^{[i]}$  in Fig. 1)

that is affordable for subsequent PT2 correction. Such a pruning step is invoked in ASCI (by retaining only a fixed number of DETs of the largest coefficients),<sup>30</sup> ACI (by enforcing that the sum of the squared coefficients of DETs is smaller than a preset threshold),<sup>27</sup> and iCIPT2 (by retaining all CSFs with coefficients larger than  $C_{\min}$  in absolute value),<sup>16</sup> but not in CIPSI,<sup>67,68</sup> SHCI,<sup>19</sup> and ICE.<sup>35</sup> While this is not very serious for CIPSI and ICE, it is not the case for SHCI due to the use of the very loose criterion (19). It has been shown<sup>17</sup> that typically 90% of the DETs selected according to the criterion (19) can be pruned away, meaning that a substantial time is wasted in the diagonalization. Speaking of the overall efficiency, the whole selection procedure with the iCI criterion (20)/(21) is about five times cheaper, whereas that with the CIPSI (17) or SHCI (19) criterion is about two times more expensive than the PT2 correction step (for more details, see Ref. 17).

The iterative selection procedure has to be terminated in one way or another. Unlike the energy convergence criterion ( $|E_1^{[i+1]} - E_1^{[i]}| \leq \epsilon$ ) adopted in the aforementioned sCI methods, the similarity between the start ( $P_0^{[i]}$ ) and pruned ( $P_2^{[i]}$ ) spaces of iteration  $i$  (see Fig. 1) is taken as the convergence check in iCIPT2, viz.

$$\frac{|P_0 [C_{\min}] \cap P_2 [C_{\min}]|}{|P_0 [C_{\min}] \cup P_2 [C_{\min}]|} \geq \tau_p \quad (22)$$

where  $\tau_p$  (=0.95) is a universal parameter.

Finally, some words on the diagonalization are necessary. As well known, the best way to make full use of the sparsity of the Hamiltonian matrix  $\mathbf{H}$  is through the matrix-vector products,  $\sigma_i = \mathbf{H}\mathbf{X}_i$ , which require only nonzero elements of  $\mathbf{H}$  (which are never stored but are recalculated whenever needed). The crucial point here is how to choose the trial (column) vectors  $\{\mathbf{X}_i\}_{i=1}^{N_b}$ , so as to expand the target roots accurately even if the space  $\mathbf{X} = \text{span}\{\mathbf{X}_i\}$  is very incomplete. Unfortunately, most schemes work with a search space  $\mathbf{X}$  whose dimension  $N_b$  increases along the iterations, thereby leading to large memory consumptions. To avoid this, iCIPT2 adopts the iterative vector interaction

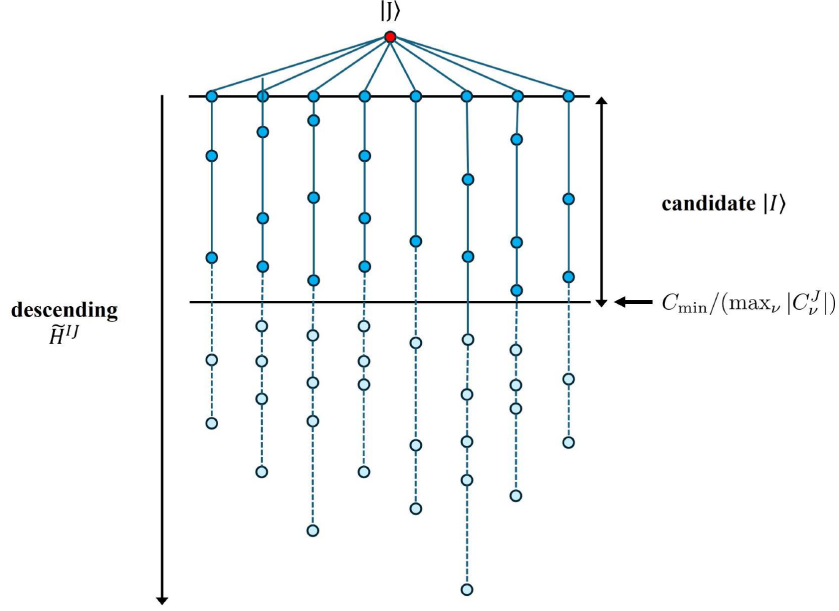


Figure 6: Screening of doubly excited configurations based on upper bounds  $\tilde{H}^{IJ}$  of Hamiltonian matrix elements.

(iVI) approach,<sup>70,71</sup> which has the following merits: (1) it adopts well defined trial vectors (by perturbation theory, intermediate Hamiltonian, conjugate gradient, etc.); (2) it works with a fixed-dimensional search space, with the dimension determined automatically by the number of target roots; (3) it can access directly interior roots without touching none of the lower roots.

## 2.5 Constraint-Based ENPT2

As long as the iteratively determined variational space  $P$  is good enough, the remaining dynamic correlation can be accounted for accurately at the lowest-order perturbation theory. To be more general, the three-space concept<sup>35,69</sup> can be adopted here. That is, the  $P$  space is split into a primary ( $P_m$ ) and a secondary ( $P_s$ ) subspace, and only the former is allowed to connect the external space  $Q = 1 - P$ . The eigenpairs  $\{\tilde{E}_k^{(0)}, |\tilde{\Psi}_k^{(0)}\rangle = \sum_{J\nu \in P_m} |J\nu\rangle C_{\nu,k}^J\}$  of the  $P_m$  space are to be corrected by ENPT2 in a state-specific manner,

viz.

$$\tilde{E}_k^{(2)}[Q] = \sum_{|I\mu\rangle \in Q} \frac{\left| \sum_{|J\nu\rangle \in P_m} H_{\mu\nu}^{IJ} C_{\nu,k}^J \right|^2}{\tilde{E}_k^{(0)} - H_{\mu\mu}^{II}} \quad (23)$$

Given its simplicity, the implementation of Eq. (23) encounters four issue:

1. How to generate efficiently the  $Q$  space, given the unstructured  $P_m$  space?
2. How to minimize the memory consumption, given the extremely large size of the  $Q$  space?
3. How to establish the connections between the oCFGs  $|I\rangle \in Q$  and those interacting oCFGs  $|J\rangle \in P_m$ ?
4. How to compute efficiently the matrix elements?

To address these issues, note first that the single and double excitations from the CSF-s/DETs of the  $P_m$  space in general span a space  $W$  that is larger than  $Q$ , for some of them may belong to  $P_m$  or  $P_s$ . That is, the net  $Q$  space can only be obtained by removing the  $P$ -space CSFs/DETs from  $W$ . However, this requires a very slow double-check process. Fortunately, this issue can be bypassed by rewriting Eq. (23) as<sup>32</sup>

$$\tilde{E}_k^{(2)}[Q] = \tilde{E}_k^{(2)}[W] - \tilde{E}_k^{(2)}[P], \quad W = P \cup Q = P_m \cup P_s \cup Q \quad (24)$$

$$\tilde{E}_k^{(2)}[W] = \sum_{|I\mu\rangle \in W} \frac{\left| \sum_{|J\nu\rangle \in P_m, |J\nu\rangle \neq |I\mu\rangle} H_{\mu\nu}^{IJ} C_{\nu,k}^J \right|^2}{\tilde{E}_k^{(0)} - H_{\mu\mu}^{II}} \quad (25)$$

$$\tilde{E}_k^{(2)}[P] = \sum_{|I\mu\rangle \in P} \frac{\left| \langle I\mu | H | \tilde{\Psi}_k^{(0)} \rangle - \langle I\mu | \tilde{\Psi}_k^{(0)} \rangle H_{\mu\mu}^{II} \right|^2}{\tilde{E}_k^{(0)} - H_{\mu\mu}^{II}} \quad (26)$$

The negative term in the numerator of Eq. (26) arises from the fact that the diagonal terms have been excluded in Eq. (25). The final energies are calculated as

$$E_k = E_k^{(0)} + \tilde{E}_k^{(2)}[Q] \quad (27)$$

where  $\{E_k^{(0)}\}$  are obtained by the diagonalization of the  $P$  space instead of the  $P_m$  space. If  $P_m$  is just the whole  $P$ , Eq. (26) can further be rewritten as

$$\tilde{E}_k^{(2)}[P] = \sum_{|I\mu\rangle \in P} \left(C_{\mu,k}^I\right)^2 \left(\tilde{E}_k^{(0)} - H_{\mu\mu}^{II}\right) \quad (28)$$

thanks to the relation  $\langle I\mu|H|\tilde{\Psi}_k^{(0)}\rangle = \tilde{E}_k^{(0)}\langle I\mu|\tilde{\Psi}_k^{(0)}\rangle = \tilde{E}_k^{(0)}C_{\mu,k}^I$  for  $\forall |I\mu\rangle \in P$ .

Inspired by the idea of constraint-based PT2,<sup>32</sup> we have developed a pipelined, constraint-based PT2 algorithm (see Fig. 7; for more details see Ref. 17):

1. Split the  $W$  space into disjoint subspaces  $\{W_i\}$  (by constraints consisting of  $L_c$  highest occupied orbitals and corresponding occupation numbers) and dynamically distribute  $\{W_i\}$  across threads or processes. Information for generating  $W_i$  is stored in a pool that is shared by all threads.
2. Picks up a subspace  $W_i$  and determine the memory to store the oCFG connection information. If  $W_i$  is too large, split it into smaller subspaces until the memory requirement is met and push those smaller subspaces back to the pool and return to Step 2.
3. Generate the oCFG connection information for each  $W_i$ . If the consumed memory does not reach the threshold, pick a new subspace and return to Step 2.
4. Sort the connection information to determine the oCFGs  $|I\rangle$  in  $W_i$  and those interacting oCFGs  $|J\rangle$  in  $P$ . Here, those doubly excited oCFGs  $|I\rangle$  with estimated upper bounds  $\tilde{H}^{IJ}$  (cf. Table 1) smaller than  $Q_{\min}/\max_{\nu,k} |C_{\nu,k}^J|$  will be deleted, so as to enhance the efficiency.
5. For each oCFG  $|I\rangle$  in  $W_i$ , allocate memory to store the numerator and denominator in Eq. (25) and generate the corresponding ROT for each connected oCFG pair  $(I, J)$ . If the memory at this step reaches a predefined threshold, then launch the calculation to get the PT2 correction from all involved oCFGs. Here, use of the sparsity of

$\mathbf{H}^{IJ}$  as well as repeated use of the BCCs and molecular integrals should be made for optimal efficiency. If the memory does not exceed the predefined threshold, then pick up a new subspace and go back to Step 2.

6. After finishing  $\tilde{E}_k^{(2)}[W]$  in Eq. (25), calculate  $\tilde{E}_k^{(2)}[P]$  in Eq. (26)/(28) and  $\tilde{E}_k^{(2)}[Q]$  in Eq. (24).

As shown in Fig. 8, the wall time of the PT2 correction scales perfectly linearly with respect to the size of  $Q$ , demonstrating the efficacy of the pipelined algorithm in memory management and massive parallelization. In particular, the algorithm is generic with respect to Hamiltonians and MPBFs.

### 3 Software Architecture

Redundant codes and repetitive tasks should be avoided as much as possible when developing an extendable and maintainable software package. Therefore, the design philosophy of MetaWave is to maximize the use of logically identical or similar functionalities. This can be achieved through C++ mechanisms such as polymorphism and template metaprogramming. Specifically, a three-layer abstract architecture (i.e., infrastructure, Hamiltonian, and wavefunction; see Fig. 9) is employed in MetaWave for furnishing a rich set of highly modular and composable functions.

#### 3.1 Infrastructure Layer

The infrastructure layer serves as the basis of MetaWave. Designed to be independent of quantum chemistry specifics, it provides a unified interface for basic linear algebra operations and algorithm templates for parallel computing, by resolving the dependency of linear algebra libraries on scalar types and the complexity of managing different parallel strategies.

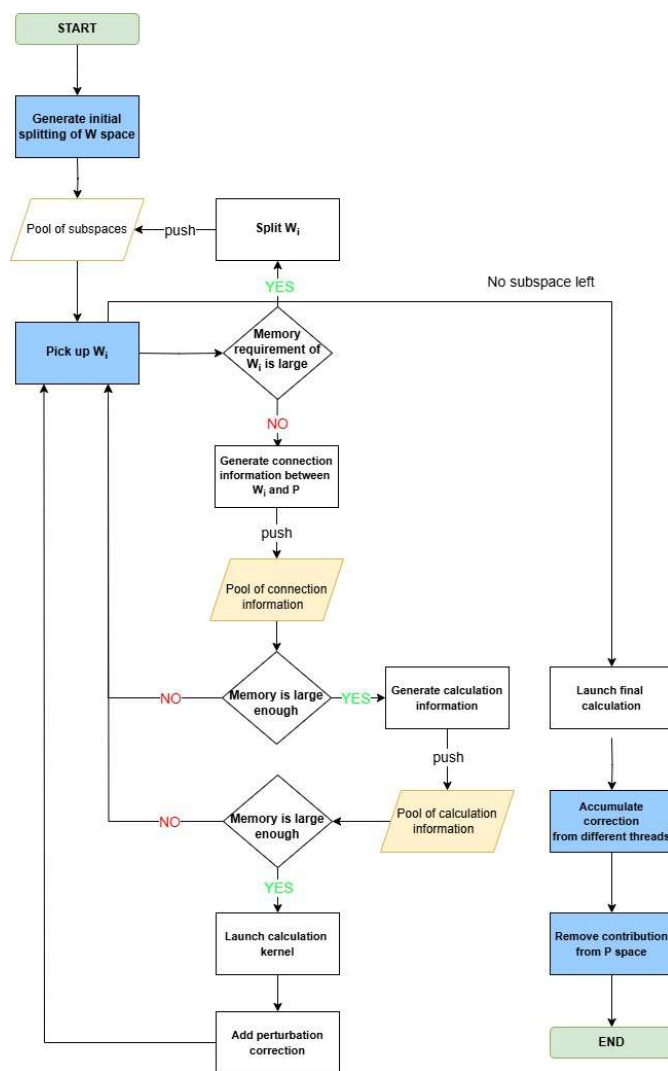


Figure 7: Workflow of pipelined, residue-based constraint-based ENPT2 in MetaWave. Green boxes represent the start and end points of the algorithm. Pool of subspaces store the those  $W_i$  that to be generated, which is shared for each thread. Yellow boxes serves as a pool for storing connection or calculation information, which is private for each thread. Connection information refers to connected oCFG pairs and calculation information refers to the ROT for each connected oCFG pair. Blue boxes indicate steps that must be executed either in single-thread mode or multi-thread mode with locks. White boxes denote steps that can be performed independently by each thread.

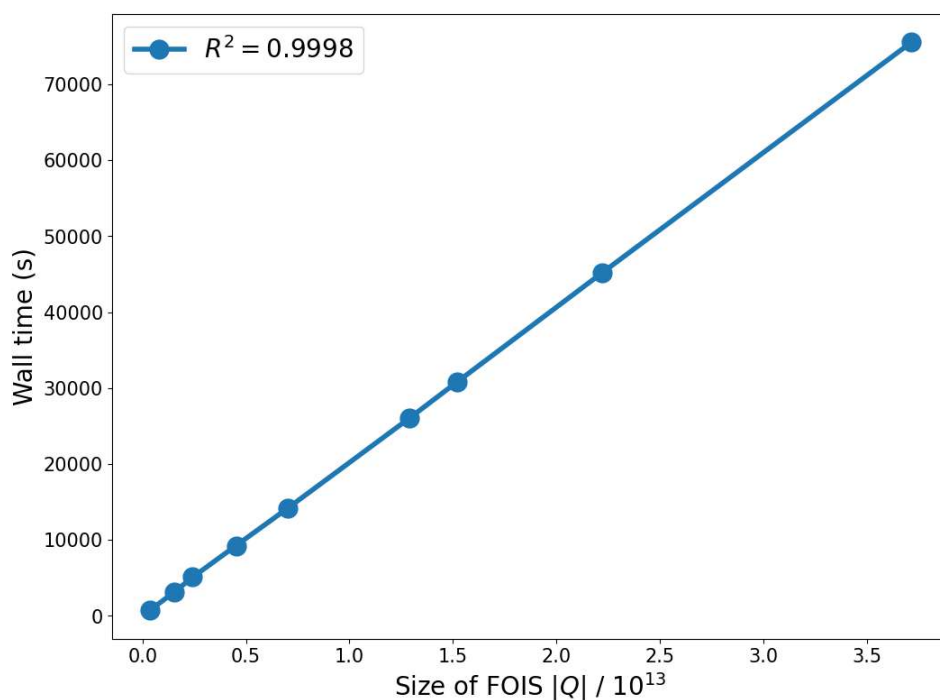


Figure 8: Wall times of the PT2 step of sf-X2C-CAS(28e,126o)-iCIPT2/cc-pVTZ-DK calculations of  $\text{Cr}_2$  as a function of the size  $|Q|$  of the first-order interaction space  $Q$ . The calculations were performed on a single node with two Hygon 7285 CPUs (32 cores, 2.0 GHz) and 512 GB of DDR4 memory.

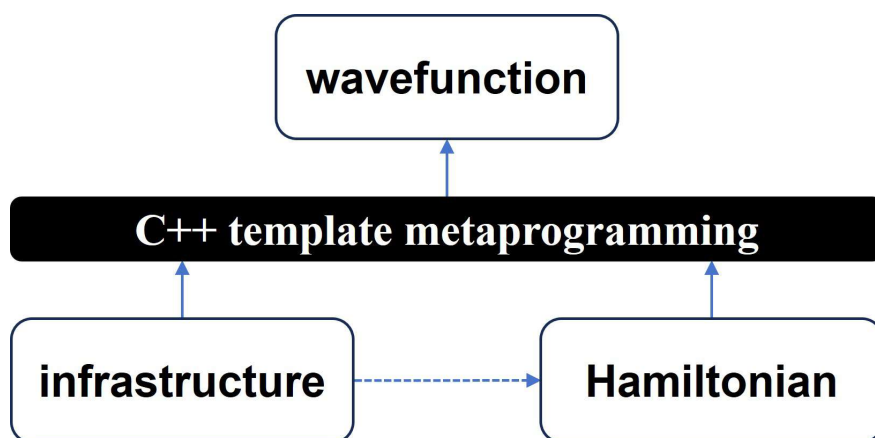


Figure 9: Three-layer architecture of MetaWave. The infrastructure layer abstracts linear algebra operations and parallelization, enabling the Hamiltonian and wavefunction layers to treat scalar types and parallel strategies as template parameters. The Hamiltonian layer encapsulates all information relevant to the Hamiltonian matrix, including molecular symmetry, MO integrals, MPBFs, and matrix element evaluation. The wavefunction layer leverages the Hamiltonian and infrastructure layers for unified implementation of relativistic and nonrelativistic many-electron wavefunctions.

### 3.1.1 Linear Algebra Interface

Linear algebra operations are fundamental to computational chemistry algorithms. Optimized libraries like BLAS (Basic Linear Algebra Subprograms) are commonly used for these operations due to their efficiency. However, BLAS functions are explicitly tied to specific scalar types, such as single-precision real (`float`), double-precision real (`double`), single-precision complex (`std::complex<float>`), and double-precision complex numbers (`std::complex<double>`). Such dependence of scalar types complicates the development of high-level codes that aim to be agnostic of the underlying data types. Take the standard BLAS function for double-precision matrix multiplication (Listing 1) as an example. In `cblas_dgemm` both the function name and parameters are specific to double-precision real numbers. To handle different scalar types, separate functions with different names and parameters are required, leading to code duplication and increased maintenance overhead. To overcome this limitation, MetaWave introduces a unified linear algebra interface that removes the dependence of scalar types. By utilizing C++ function overloading and templates, we provided a set of functions where the same function name can operate on different scalar types. This allows high-level codes to perform linear algebra operations without concern for the underlying data types.

Listing 1: Declaration of `cblas_dgemm`.

```
1 void cblas_dgemm(const CBLAS_LAYOUT Layout ,
2                 const CBLAS_TRANSPOSE transa ,
3                 const CBLAS_TRANSPOSE transb ,
4                 const MKL_INT m, const MKL_INT n, const MKL_INT k ,
5                 const double alpha, const double *a, const MKL_INT lda ,
6                 const double *b, const MKL_INT ldb, const double beta ,
7                 double *c, const MKL_INT ldc);
```

This unification is particularly important because nonrelativistic quantum chemical calculations typically involve real numbers, whereas relativistic calculations require com-

plex numbers. By abstracting the scalar types, we laid the groundwork for a Hamiltonian-agnostic implementation, allowing the same high-level code to operate seamlessly on different types of Hamiltonians.

### 3.1.2 Parallel Algorithm Template

Efficient parallel computing is crucial for the execution of wavefunction methods. However, managing parallelism, particularly across various strategies such as OpenMP and MPI, can be complex and error-prone. Explicitly addressing these details in each algorithm module results in code duplication and heightens the risk of bugs. To tackle this challenge, MetaWave utilizes algorithm templates that encapsulate the parallelization logic.

For OpenMP, we provided a base class `OpenMPAlgorithmBase` that defines several generic parallel execution patterns using OpenMP. This approach allows developers to focus on the algorithmic implementation rather than the intricacies of parallelization, enhancing code cleaning and reducing maintenance overhead. For example, in task-based parallel strategy, the core function of the generic algorithm template is the `Run()` method (Listing 2).

Listing 2: OpenMP parallel algorithm template in MetaWave.

```
1 inline void OpenMPAlgorithmBase::Run(){
2     build_needed_info();
3     omp_schedule_init();
4     #pragma omp parallel num_threads(num_of_threads)
5     {
6         thread_init();
7         #pragma omp for schedule(dynamic, 1) nowait
8         for (size_t i = begin_idx; i < end_idx; ++i){
9             do_task(i);}
}
```

```
10         thread_finalize();
11     }
12     omp_merge_data();
13 }
```

By inheriting from `OpenMPAlgorithmBase` and implementing virtual functions (e.g., `build_needed_info()`, `omp_schedule_init()`, `thread_init()`, `do_task(i)`, `thread_finalize()`, and `omp_merge_data()`), developers can create new algorithm modules without directly managing the parallelization details. This design promotes code reuse and consistency across different modules, making the codebase more maintainable and less error-prone.

An additional advantage of this approach is the straightforward extension of OpenMP to MPI, by providing an MPI-specific implementation of the base class and developing a functor that maps each OpenMP-based algorithm to its MPI-based equivalent. Specifically, two issues have to be addressed:

1. How to schedule tasks on different nodes to keep load balance?
2. How to extend shared memory algorithm to distributed memory algorithm?

For the first issue, it is worth noting that OpenMP algorithms rely on built-in dynamic load balancing for loops, but MPI lacks similar functionality. To maximize parallel efficiency, we designed a double-layer dynamic task schedule framework involving both MPI and OpenMP. A unique MPI scheduler on the root process packages for-loop tasks into chunks and dispatches them dynamically to worker nodes. The scheduler monitors worker statuses and assigns the next chunk to the first available node. Each worker unpacks the chunk and processes it using the original OpenMP algorithm. After completing the chunk, the worker signals completion and receives the next chunk. This approach achieves efficient load balancing without algorithm-specific settings and allows the program to adjust dynamically to runtime conditions, such as variations in computation times and hardware differences. Thus, the generic MPI dynamic schedule is devised

into two parts, the MPI scheduler (Listing 3) and work nodes (Listing 4).

Listing 3: Scheduler-side code for MPI dynamic scheduling in MetaWave.

```
1 for (size_t chunk_id = 0; chunk_id < chunk_num; chunk_id++){
2     MPI_Waitany_process(); // check if any process returns
3     MPI_Send_chunk();     // send chunk to idle process
4 }
5 MPI_Waitall_finish(); // wait for all process finish
6 MPI_Send_stop_signal(); // send stop signal to workers
```

Listing 4: Work nodes code for MPI dynamic scheduling in MetaWave.

```
1 while(true){
2     MPI_Recv()
3     if (Recv_calc_signal()) // start another original OpenMP
4         calculation
5     {
6         Run_OpenMP();
7     }
8     else if (Recv_stop_signal()) // this worker should stop
9     {
10        break;
11    }
12    else
13    {
14        throw std::runtime_error();
15    }
16 }
```

We also employed techniques like preserving thread context between OpenMP cycles and double-layer parallel data merging to optimize the MPI-OpenMP calculations. Detailed

descriptions of these optimizations will be presented elsewhere.

As for the second issue, we optimized memory usage by utilizing the serialization and memory pool techniques. MPI communication typically requires contiguous memory, but data structures in MetaWave are automatically generated through inheritance, template combination, and specialization, resulting in complex, non-contiguous memory layouts. To resolve this, we adopted a serialization approach using the cereal library<sup>72</sup> for serialization and deserialization. By specifying which class members require serialization, we wrapped MPI functions into template functions that handle serialized streams. This allows our complex data structures to be transmitted over MPI interfaces seamlessly. Consequently, any class with specified serializable members can be used with common MPI functions like `MPI_Recv()` and `MPI_Bcast()` automatically.

The use of a memory pool is to control memory usage and facilitate data reuse via pre-allocating large chunks of memory. This technique is inherently compatible with MPI. We categorized memory usage in MetaWave into static memory and dynamic memory managed by the memory pool. The former is required to store basic information (e.g., configuration spaces) of the program, while the latter refers to intermediate data structures (e.g., ROTs and various records used in the ranking and perturbation steps). In our MPI implementation, the static memory is not distributed; all nodes store a copy. The intermediate data structures in the memory pool are generated from dynamically distributed chunks, which naturally form a distributed memory structure without the need for manual intervention. This approach optimizes memory usage and enhances performance in distributed computing environments.

As a demonstration of our MPI implementation, we performed CAS(28e,126o)-iCIPT2 calculations on  $\text{Cr}_2$  using the spin-free (sf) part<sup>73,74</sup> of the exact two-component (X2C) Hamiltonian<sup>75,76</sup> and the cc-pVTZ-DK basis set.<sup>77</sup> There are  $2.0 \times 10^7$  CSFs in the variational space with  $C_{\min} = 7 \times 10^{-6}$  for the control of selection. It can be seen from Fig. 10 that our MPI implementation of the PT2 step achieved 94.0% parallel efficiency for 16

nodes (each of which has two Hygon 7285 CPUs (32 cores, 2.0 GHZ) and 512 GB DDR4 memory).

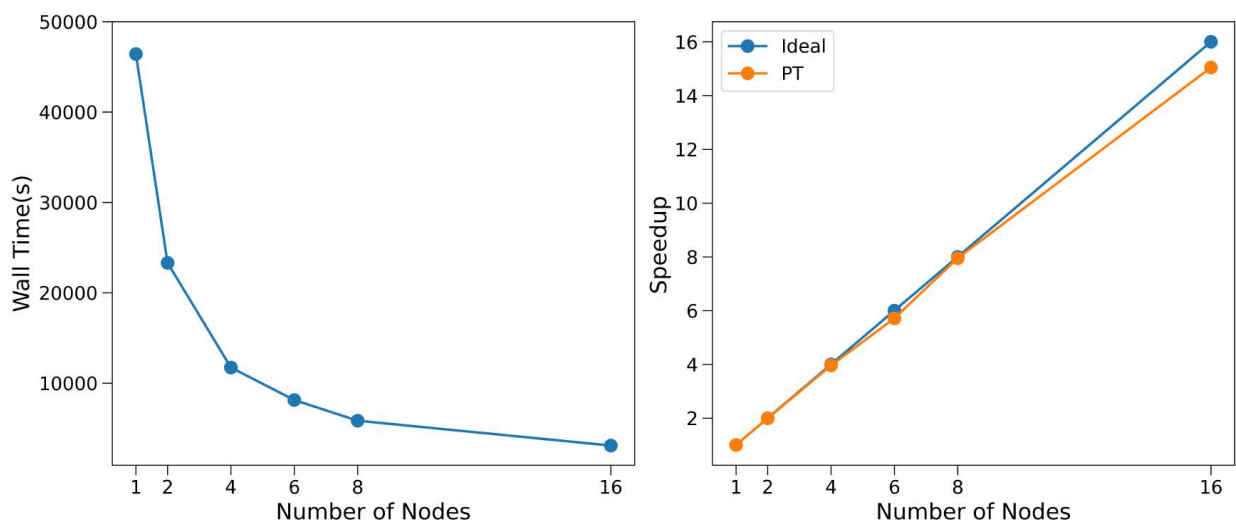


Figure 10: Wall times (left) and speedups (right) for the PT2 step [ $E^{(2)} = -0.088495 E_h$ ] of sf-X2C-CAS(28e,126o)-iCIPT2[ $C_{\min} = 7 \times 10^{-6}$ ]/cc-pVTZ-DK calculations of  $\text{Cr}_2$  on up to 16 nodes. Each node contains two Hygon 7285 CPUs (32 cores, 2.0 GHZ) and 512 GB DDR4 memory. The variational space contains  $2.0 \times 10^7$  CSFs. 94.0% parallel efficiency is achieved for 16 nodes.

### 3.2 Hamiltonian Layer

The Hamiltonian layer serves as the core of MetaWave and is responsible for handling domain-specific components such as Hamiltonian, MPBFs, (abelian) spatial symmetry, (non-abelian) spin symmetry, molecular integrals, and matrix element evaluation. It creates a flexible and extensible framework that can be reused across different quantum chemical methods. A key feature of this layer is the use of a type-trait and tagging system,

which allows for the unified handling of various Hamiltonians, molecular symmetries, and MPBFs. By passing information through template parameters and utilizing compile-time mechanisms, both duplication reduction and maintainability enhancement can be achieved. Furthermore, compile-time optimization is also facilitated in this way.

### 3.2.1 Type-Trait and Tagging System

To achieve flexibility and extensibility, MetaWave employs a type-trait and tagging system. This system encodes properties of different Hamiltonians, molecular symmetries, and MPBFs at compile time, allowing the compiler to generate optimized code. As a result, this type-trait and tagging system allows us to write generic code that adapts to different Hamiltonians without code duplication, in the same spirit as other codes.<sup>45,78–80</sup>

A tag is implemented using an empty struct that serve as a unique type representing the specific concept. For example, tags for different Hamiltonians are defined in Listing 5, where `ElectronNonRela` and `ElectronRela` represent the electron-only nonrelativistic and relativistic Hamiltonians, respectively, while `Hubbard` represents the Hubbard model Hamiltonian. These tags are used as template parameters to differentiate between Hamiltonian types in a type-safe manner.

Listing 5: Hamiltonian tag system in MetaWave.

```
1 namespace tag {  
2     namespace Hamiltonian {  
3         struct ElectronNonRela{};  
4         struct ElectronRela{};  
5         struct Hubbard{};  
6     };  
7 };
```

To associate properties with these tags, we used type-traits structures (helper classes) that provide compile-time information about the Hamiltonian's characteristics (Listing

6).

Listing 6: Hamiltonian type-traits system in MetaWave.

```
1 namespace trait {
2   template <typename HamiltonianTy>
3     struct hamiltonian_property;
4
5   template <>
6     struct hamiltonian_property<tag::Hamiltonian::ElectronNonRela>
7     {
8         static constexpr bool has_twobody_term = true;
9         static constexpr bool has_onebody_term = true;
10        static constexpr bool has_oneext_term = true;
11        static constexpr bool has_twoext_term = true;
12    };
13
14   template <>
15     struct hamiltonian_property<tag::Hamiltonian::Hubbard>
16     {
17        static constexpr bool has_twobody_term = true;
18        static constexpr bool has_onebody_term = true;
19        static constexpr bool has_oneext_term = true;
20        static constexpr bool has_twoext_term = false;
21    };
22 };
```

These structures specify whether the Hamiltonian includes certain terms, such as the one-body  $H_1^0 + H_1^1$  and two-body  $H_2^0 + H_2^1 + H_2^2$  terms. To facilitate easy access to these properties, we introduced the metafunctions<sup>3</sup> (Listing 7).

---

<sup>3</sup>A metafunction is a function or operation that works at compile time rather than at runtime. In C++

Listing 7: Hamiltonian metafunctions in MetaWave.

```

1 namespace metafunc {
2
3     template <typename HamiltonianTy>
4     inline static constexpr bool has_twobody_term_v = trait::
        hamiltonian_property<Hamiltonian_t>::has_twobody_term;
5
6     template <typename HamiltonianTy>
7     inline static constexpr bool has_onebody_term_v = trait::
        hamiltonian_property<Hamiltonian_t>::has_onebody_term;
8
9     template <typename HamiltonianTy>
10    inline static constexpr bool has_oneext_term_v = trait::
        hamiltonian_property<Hamiltonian_t>::has_oneext_term;
11
12    template <typename HamiltonianTy>
13    inline static constexpr bool has_twoext_term_v = trait::
        hamiltonian_property<Hamiltonian_t>::has_twoext_term;
14 };

```

These compile-time constants can be used within templates to enable or disable code paths, ensuring that only relevant computations are performed for a given Hamiltonian type. For example, for the Hubbard model, all the code paths related to the evaluation of matrix elements between doubly excited configurations can be ignored, leading to a more efficient implementation. Moreover, by utilizing the type-trait and tagging system, both spatial and spin symmetries can be readily be handled. As shown in Fig. 11, symmetry adaptation improves significantly the compactness of the variational wavefunctions in

---

programming, especially in template metaprogramming, metafunctions are used to perform computations, checks, or transformations on types and constants at compile time. This allows the compiler to make decisions and optimize code before it runs, which can lead to more efficient and flexible programs.

selected iCI (SiCI) calculations. Stated differently, on average, a symmetry adapted MPBF tends to contribute more to correlation than the unadapted one (see also Ref. 35).

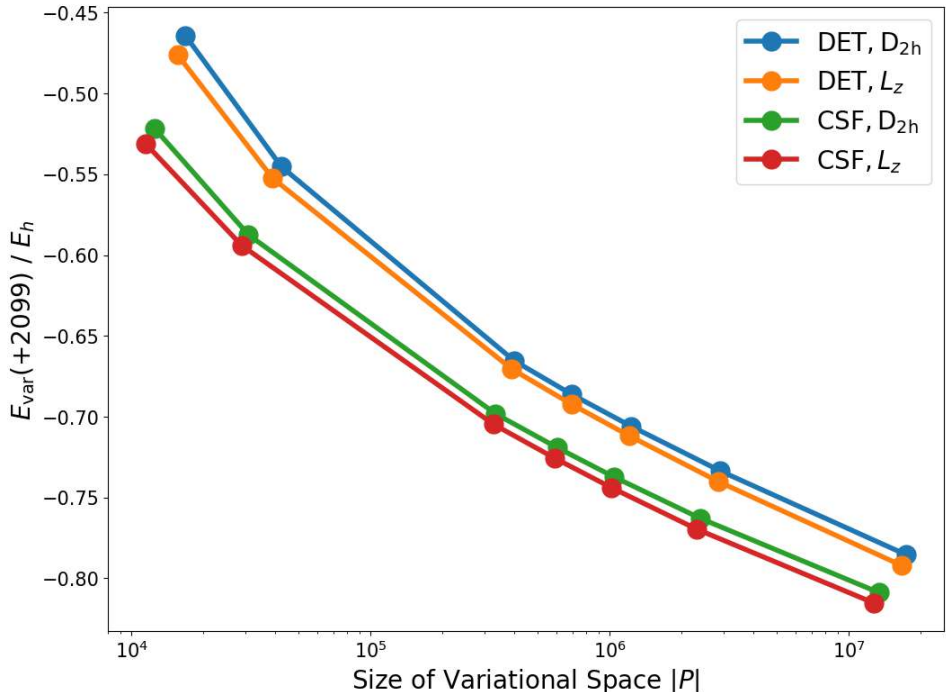


Figure 11: sf-X2C-CAS(28e,76o)-SiCI/cc-pVDZ-DK results for  $\text{Cr}_2$  with different symmetries.

The type-trait and tagging system also helps to automatically generate a large number of functions with similar computational processes. Consider, e.g., the BCCs  $\langle \tilde{I}\mu | e_{\tilde{i}\tilde{j},\tilde{k}\tilde{l}} | \tilde{J}\nu \rangle$  of the reduced oCFG pair  $(\tilde{I}, \tilde{J})$ . They involve segment values of all spatial orbitals, under the restriction that outside the interaction region,  $[\min(\tilde{i}, \tilde{j}, \tilde{k}, \tilde{l}), \max(\tilde{i}, \tilde{j}, \tilde{k}, \tilde{l})]$ , of the operator  $e_{\tilde{i}\tilde{j},\tilde{k}\tilde{l}}$ , the bra and ket orbitals and their occupations should be the same. The problem lies in that there are seven different types of ROTs and various segment types (cf. Table 2 in Ref. 16). It is extremely tedious and error-prone to write each case individually. This is avoided in MetaWave by using template functions, where each involved component is determined automatically via the corresponding type-trait and tagging system designed for UGA.

Take the function (Listing 8) for generating the BCCs between doubly excited oCFG pair  $(\tilde{I}, \tilde{J})$  as an example. Given the input parameter `csf_idx` (which corresponds to  $\nu$ ), it

generates all non-vanishing BCCs  $\langle \tilde{I}\mu | e_{\tilde{i}\tilde{j},\tilde{k}\tilde{l}} | \tilde{J}\nu \rangle$  and store the results and the indices  $\mu$  in `drct` and `indx` respectively. If exists, the function also generates  $\langle \tilde{I}\mu | e_{\tilde{i}\tilde{l},\tilde{k}\tilde{j}} | \tilde{J}\nu \rangle$  and stores it in `xchng`. Since the number of CSFs that one oCFG can generate cannot exceed the range of `int32_t` in routine applications, `int32_t` is used to represent the indices  $\mu$  and  $\nu$ . In `maketable_dbl`, `_init_propagate` and `_final_propagate` correspond to the evaluation outside the interaction region, while the other functions handle the evaluation within each region. Specifically, `_propagate_segment2` evaluates the orbitals where the operators act, whereas `_propagate_segment1` evaluates those where no operator acts. To determine the correct segment value, each function takes `TableTy` as one of the template parameters and uses the corresponding type-traits for `TableTy`, along with internal information contained in the class `TUGATableMaker`. The number specified as the second template parameter distinguishes different regions for a given operator.

Listing 8: Template function for generating BCCs between doubly excited oCFG pairs.

```

1 template <typename TableTy>
2 inline int32_t TUGATableMaker::maketable_dbl(const int32_t csfindx,
        double *drct, double *xchng, int32_t *indx)
3 {
4     if (_init_propagate<TableTy>(csfindx) == false)
5     {
6         return 0;
7     }
8
9     _propagate_segment2<TableTy, 0>();
10    _propagate_segment1<TableTy, 1>();
11    _propagate_segment2<TableTy, 1>();
12    _propagate_segment1<TableTy, 2>();
13    _propagate_segment2<TableTy, 2>();
14    _propagate_segment1<TableTy, 3>();

```

```

15     _propagate_segment2<TableTy, 3>();
16
17     return _final_propagate<TableTy>(csfindx, drct, xchng, indx);
18 }

```

Labeling specific concepts via empty structs and extracting/accessing properties via type traiting/metafuncions have been employed in all aspects of MetaWave, from the lowest infrastructure layer to the highest wavefunction layer. This is the essential trick that makes each component independent and the coding as generic as possible.

### 3.2.2 Configuration Space

The CfgSpace class in MetaWave is a central component that manages both the MPBFs and CI vectors. It is determined by 4 template parameters:

1. SymTy : type of spatial symmetry;
2. IndxTy : type used to store the indices  $\mu$  of  $|I\mu\rangle$ ;
3. BasisTy : type of MPBFs (CSF or DET);
4. ScalarTy : scalar type of CI vectors (e.g. `double`, `std::complex<double>`).

The first two parameters are related to oCFGs and are hence encapsulated in the BasisMetadata class (Listing 9) to represent the MPBFs. This class stores the essential information of each MPBF, including spin information ( $2S$  for CSFs and  $2S_z$  for DETs), number of open-shell electrons, irreducible representations (irrep), a pointer to the string that stores the oCFG, and CSF/DET indices.

Listing 9: Definition of class BasisMetadata representing the MPBFs.

```

1 template <typename SymTy, typename IndxTy>
2 class BasisMetadata
3 {

```

```

4     public:
5     /* typedef */
6     using indx_t = IndxTy;
7     using sym_t  = SymTy;
8     /// .... omitted
9     protected:
10    int8_t      spintwo_or_sztwo, nopen;
11    SymTy      irrep;
12    uint64_t*  oCFG;
13    IndxTy     indx;
14 };

```

The BasisManager class (Listing 10) manages a collection of BasisMetadata instances. It provides functionalities for handling MPBFs, such as adding CSFs/DETs, extracting information from a given CSF/DET, or sorting the MPBFs to canonical form. This class is uniform for CSFs and DETs.

Listing 10: Definition of class BasisManager.

```

1 template <typename BasisMetadataTy>
2 class BasisManager
3 {
4     public:
5     /* typedef */
6
7     using sym_t  = typename BasisMetadataTy::sym_t;
8     using indx_t = typename BasisMetadataTy::indx_t;
9     using metadata_t = BasisMetadataTy;
10    using iter_t = typename std::vector<BasisMetadataTy>::
        iterator;
11

```

```

12     /* functions */
13     void add_basis(std::vector<int8_t>& Occ, uint32_t norb,
14                 uint32_t spintwo, uint32_t _indx);
15     void extract_info_given_basis(const uint32_t id, uint64_t*
16                                 OccCode);
17     template <class CompareFuncTy>
18     void sort();
19     virtual void build();
20     /// .... omitted
21 };

```

Finally, the CfgSpace class (Listing 11) represents the entire configuration space, managing both the configurations and the associated CI vectors. In CfgSpace, the key types, scalar\_t, sym\_t, indx\_t, and others, are determined by the template parameters and propagated via the using declarations. This design ensures that the configuration space is aware of the types used in both the basis manager and vector manager, providing the necessary flexibility for the entire algorithm. The use of template parameters and type binding allows for generic programming, reducing code duplication and enhancing maintainability.

Listing 11: Definition of class CfgSpace.

```

1 template <class BasisManagerTy, class VecManagerTy, typename BasisTy>
2 class CfgSpace
3 {
4     public:
5
6     /* typedef */
7
8     using scalar_t = typename VecManagerTy::scalar_t;

```

```

9     using sym_t      = typename BasisManagerTy::sym_t;
10    using indx_t     = typename BasisManagerTy::indx_t;
11    using metadata_t = typename BasisManagerTy::metadata_t;
12    using iter_t     = typename BasisManagerTy::iter_t;
13    using basis_t    = BasisTy; // DET or CSF
14
15    /// .... omitted
16 }:
```

MetaWave also provides numerous functions, such as printing for debugging purposes, dumping data for restarting computations, merging two configuration spaces, and more. These functionalities enhance the usability and robustness of the MetaWave package, allowing users to efficiently manage and manipulate the configuration space as needed.

### 3.2.3 Integral Manager

The `IntegralManager` class is responsible for handling molecular integrals. The main challenge is how to deal with different kinds of permutation and single/double point group symmetries. In the spin-free case, the two-electron integrals exhibit 8-fold permutation symmetry and are real; for systems with  $L_z$  symmetry, this symmetry is reduced to 4-fold, but the integrals still remain real. In the spin-dependent case, the integrals (over spinors) are generally complex with complicated permutation and double point group symmetries.<sup>7</sup> Hence, permutation and single/double point group symmetries are not uncorrelated. To store and retrieve different kinds of molecular integrals in a uniform manner, we used a tag system to label different permutation symmetries (Listing 12) and a metafunction `perm_symm_t` to map each single/double group irrep to the corresponding permutation symmetry for molecular integrals at compile time.

Listing 12: Tag system to label permutation symmetries.

```

1 namespace tag {
```

```

2     namespace Integrals {
3         struct PermutationSymmetry
4         {
5             struct Fold8 {};
6             struct Fold4 {};
7             /// ..... omitted
8         }
9     }
10 };

```

The skeleton code for the `IntegralManager` class is shown in Listing 13. The template parameters `ScalarTy` and `perm_symm_t<SymTy>` of `VectorStorage` specify scalar type (real or complex) and permutation symmetry of the integrals, respectively. Note in passing that point group symmetries are not employed here for storage reduction, simply because all integrals can be stored in memory after accounting for permutation symmetries (for the number of correlated orbitals is usually much less 1000). Yet, point group symmetries are indeed ensured by the `get_1b` and `get_2b` functions, which return zeros when the direct product of the irreps of the input orbitals does not contain the trivial irrep. With this design, the C++ compiler can use the tagging and type-trait system to synthesize the correct data structures for storing the molecular integrals at compile time. This allows the programmer to write a uniform code without the need to consider the permutation symmetry explicitly.

Listing 13: Skeleton of class `IntegralManager`.

```

1 template <typename ScalarTy, typename SymTy>
2 class IntegralManager
3 {
4     public:
5

```

```

6      /* function */
7
8      virtual ScalarTy get_1b(const unsigned p, const unsigned q)
          const
9      {
10         return integrals_1b(p,q);
11     }
12     virtual ScalarTy get_2b(const unsigned p, const unsigned q,
          const unsigned r, const unsigned s) const
13     {
14         return integrals_2b(p,q,r,s);
15     }
16
17     /// .... omitted
18
19     protected:
20
21     /* storage */
22
23     VectorStorage<ScalarTy, perm_symm_t<SymTy>> integrals_1b;
24     VectorStorage<ScalarTy, perm_symm_t<SymTy>> integrals_2b;
25
26     /// .... omitted
27 };

```

### 3.2.4 Evaluation of HMEs

In MetaWave, the calculation of HMEs involves several steps. The general workflow begins with the classification of oCFG pairs and generation of the corresponding reduced oCFG

pairs. This is followed by retrieving the necessary integrals, computing the BCCs, and finally contracting these components to obtain the HMEs. Due to the complexity and intricacy of the algorithms involved in these steps, we do not delve into details here. Instead, we emphasize that MetaWave provides kernel-level template functions for each step, which can be utilized by higher-level algorithms. For example, for singly excited oCFG pairs, we have several functions shown in Listing 14. This modular design allows for flexibility and reusability, making it easier to maintain and extend the codebase.

Listing 14: Functions for evaluation of HMEs between singly excited oCFG pairs.

```

1 template <typename TableTy>
2 inline void _generate_table_sngl(const uint64_t* BraCFG, const
   uint64_t* KetCFG, const int LenCode,
3 TableTy* Table, tag::Hamiltonian::ElectronNonRela);
4
5 template <typename TableTy>
6 inline void _generate_table_sngl(const uint64_t* BraCFG, const
   uint64_t* KetCFG, const int LenCode,
7 TableTy* Table, tag::Hamiltonian::ElectronRela);
8
9 template <typename TableTy, typename IntegralsTy>
10 inline void _fetch_ints_sngl(TableTy* Table, const IntegralsTy*
   Integrals, tag::Hamiltonian::ElectronNonRela);
11
12 template <typename TableInfoTransferTy, typename IntegralsTy>
13 inline void _fetch_ints_sngl(TableTy* Table, const IntegralsTy*
   Integrals, tag::Hamiltonian::ElectronRela);

```

An important aspect of our implementation is the accommodation of different Hamiltonians. Different Hamiltonians correspond to distinct molecular integrals, which have different permutation symmetries, and therefore different storage requirements, neces-

sitating specialized implementations for each. To handle this variety without code duplication, MetaWave employs a technique known as tag dispatching, where specific types (tags) are used to direct the compiler to appropriate function implementations at compile time via function overloading. For instance, the last parameter in the functions `_generate_table_sngl` and `_fetch_ints_sngl` is a tag that specifies the type of Hamiltonian, which allows the compiler to pick up automatically the right Hamiltonian.

### 3.3 Wavefunction Layer

The wavefunction layer is the highest level in the MetaWave architecture. It employs the classes defined in the Hamiltonian layer as template parameters to generate the corresponding algorithm modules, such as selection and perturbation (see Sec. 2). These algorithm classes follow a consistent pattern: First, each algorithm is encapsulated in a class (typically ending with `ThreadContext`) that describes the tasks to be performed by a single thread. For instance, in the ranking step of the selection process, the `RankingThreadContext` class is invoked to generate important excited CSFs/DETs from a reference CSF/DET. In the PT2 module, a similar class handles the calculation of the PT2 correction from a specific subspace  $W_i$ . Second, parallelization is achieved through parallel templates that describe how to distribute and manage tasks across multiple threads or processes. For OpenMP, these algorithm classes inherit from a base class (e.g., `OpenMPAlgorithmBase` described above) and implement the necessary functions to assign tasks to each thread and merge the results efficiently. An important aspect of our design is the implementation of MPI: The same OpenMP parallel algorithm classes are inherited, with suitable modifications of the relevant functions to create an automatic mapping functor from OpenMP to MPI. Since the sCI algorithms can be designed such that subtasks are independent of each other and require no communication (aside from dynamic scheduling) during execution—only data merging in the end, this functor can effectively distribute tasks across MPI processes. Separating MPI from the single-threaded algorithms ensures that the core

algorithm logic remains unchanged while parallelism is handled independently. Specific implementation of the wavefunction layer is skipped here, as it would largely repeat the content already covered in Sec. 2.

### 3.4 Overview of MetaWave Functionality

MetaWave offers a comprehensive suite of features designed to facilitate the development of quantum chemical methods. The key functionalities currently supported by MetaWave include:

#### 1. Hamiltonian:

- Nonrelativistic Hamiltonian: iCIPT2<sup>16,17</sup>
  - Spin symmetry;
  - Spatial symmetry:
    - \* Binary point group symmetry;
    - \*  $L_z$  symmetry;
    - \* Translation symmetry (1D, 2D, and 3D);
- spin-separated X2C Hamiltonian:<sup>73,74</sup> SOiCI and iCISO<sup>36</sup>
  - Time reversal symmetry;
  - Binary double point group symmetry;
- Relativistic Hamiltonians: 4C-iCIPT2<sup>7</sup>
  - Time reversal symmetry;
  - Binary double point group symmetry;
- Hubbard model:
  - Nearest and next nearest hopping terms;
  - 1D, 2D, and 3D;

- Open and periodic boundary conditions.

## 2. Density Matrices:

- Reduced density matrices up to fourth order;
- Transition density matrices up to second order;
- Spin density matrices up to second order.

3. **Natural Orbitals** from spin-adapted first-order density matrix;

4. **Core-Valence Separation** for core excited and ionized states;

## 5. Parallelization:

- OpenMP
- MPI

# 4 Application

MetaWave has served as the platform for the development of spin-free<sup>16,17</sup> and spin-dependent<sup>7,36</sup> iCIPT2, which can be applied to both core and valence states of challenging systems, especially for benchmarking purposes.<sup>81–83</sup> Taking iCIPT2 as the solver of CASSCF, we obtain iCISCF(2)<sup>18</sup> and SOiCISCF(2),<sup>37</sup> where the symbol '(2)' implies that the PT2 corrections are only performed within the active space. iCISCF(2) can handle active spaces as large as (60e,60o), on top of which spin-orbit coupling can further be treated variationally by SOiCISCF(2).

Instead of real applications, a direct comparison of sf-X2C-iCIPT2, SOiCI, and 4C-iCIPT2 (which are based on the sf-X2C, sf-X2C+so-DKH1,<sup>73,74</sup> and DCB Hamiltonians, respectively) is more relevant in the present context, for they share the same infrastructure, such that their relative efficiency reflects directly the efficacy of MetaWave. To this end, the

bromine atom is enough for a showcase. The uncontracted cc-pVXZ-DK (X=D, T, Q) basis sets<sup>84,85</sup> were used. Keeping the Ar-core frozen, the three basis sets give rise to correlation spaces (17e, 68o), (17e, 102o), and (17e, 143o), respectively, for both sf-X2C-iCIPT2 and SOiCI, whereas to (17e, 136o), (17e, 204o), and (17e, 286o), respectively, for 4C-iCIPT2. The orbitals for sf-X2C-iCIPT2 and SOiCI were generated by a state-averaged CASSCF(5e,3o) calculation, whereas the spinors for 4C-iCIPT2 were generated from the Dirac-Hartree-Fock calculation of Br<sup>-</sup> (to avoid symmetry breaking). In the sf-X2C-iCIPT2 calculations, the three components of the ground state  $^2P$  are evenly distributed in the  $B_{1u}$ ,  $B_{2u}$ , and  $B_{3u}$  irreps of  $D_{2h}$ , whereas in the SOiCI and 4C-iCIPT2 calculations, the use of time reversal symmetry reduces the number of states from 6 ( $^2P_{j,m_j}$ ,  $j = 1/2, 3/2$ ,  $m_j \in [-j, j]$ ) to 3 ( $^2P_{j,|m_j|}$ ) in the  $E_{1/2}$  irrep of  $D_{2h}^*$ . The so-calculated spin-orbit splittings (SOS) of the  $^2P$  state of Br are presented in Table 2, to be compared with the experimental value<sup>86</sup> of 3685 cm<sup>-1</sup>.

In principle, the costs of the ranking, pruning, and PT2 steps of the three methods should be compared separately. However, the costs for the ranking and pruning steps exhibit considerable variations due to several factors: (1) the number of iterations, including the macro-cycles of ranking and pruning as well as the micro-cycles of diagonalization, may differ significantly; (2) the ranking step is governed predominantly by non-computational operations such as memory allocation and sorting; (3) even the computational operations are memory-bound (meaning that their performance depends on data retrieval from cache/memory) and cannot fully explore the data locality in practice. Consequently, the running environment of the computer system may impact significantly the performance of these operations. As a result, it is not meaningful to compare the costs for the ranking and pruning steps of different methods. In contrast, the PT2 step is much less affected by environmental factors. In particular, it dominates the overall computational cost as the size of the variational space grows. Therefore, it is more appropriate to compare the PT2 wall times ( $T_2$ ) in the sf-X2C-iCIPT, SOiCI, and 4C-iCIPT2 calcula-

tions. The results are documented in Table 3, along with the sizes  $|P|$  of the variational spaces for the selection thresholds  $C_{\min} = \{5.0, 3.0, 1.5, 0.9, 0.5\} \times 10^{-5}$ . It is first noted that the PT2 steps of all the methods scale linearly with respect to the sizes of the variational spaces (cf. Table 4). The PT2 step of SOiCI turns out to be about 1.5  $\sim$  2 times that of sf-X2C-iCIPT2. This can be understood as follows. If the additional selection of singly excited CSFs by the effective one-body spin-orbit coupling (SOC) operator (so-DKH1<sup>73,74</sup>) is not to be performed after the selection of sf-X2C-iCIPT2, the PT2 step of SOiCI would precisely double that of sf-X2C-iCIPT2, due to the doubled size of the variational space (i.e.,  $2S + 1 = 2$  times  $|P|$  of sf-X2C-iCIPT2). In the case of Br, only a small number of quartet CSFs is brought into the variational space of SOiCI due to the additional SOC selection. Therefore, the fact that the PT2 step of SOiCI can be less than double that of sf-X2C-iCIPT2 must stem from the better data vectorization in the case of SOiCI, which treats the three states simultaneously rather than individually as done by sf-X2C-iCIPT2. In contrast, the PT2 step of 4C-iCIPT2 is typically 10  $\sim$  15 times that of SOiCI, due to changes in the natures of MPBFs and Hamiltonian.

Table 2: Energies (in  $E_h$ ) of  ${}^2P$ ,  ${}^2P_{3/2}$ , and  ${}^2P_{1/2}$  of Br Calculated by sf-X2C-iCIPT2, SOiCI, and 4C-iCIPT2 with Uncontracted cc-pVXZ-DK (X=D,T,Q) Basis Sets.

Basis	$C_{\min}$	sf-X2C-iCIPT2		SOiCI		4C-iCIPT2		SOS*	
		${}^2P$	${}^2P_{3/2}$	${}^2P_{1/2}$	${}^2P_{3/2}$	${}^2P_{1/2}$	${}^2P_{3/2}$	${}^2P_{1/2}$	SOiCI
DZ	$5.0 \times 10^{-5}$	-2604.714234	-2604.722759	-2604.706763	-2603.932931	-2603.916402	3511	3628	
	$3.0 \times 10^{-5}$	-2604.714149	-2604.722688	-2604.706685	-2603.932466	-2603.916013	3512	3611	
	$1.5 \times 10^{-5}$	-2604.713998	-2604.722550	-2604.706540	-2603.931715	-2603.915262	3514	3611	
	$9.0 \times 10^{-6}$	-2604.713921	-2604.722478	-2604.706465	-2603.931695	-2603.915244	3514	3611	
	$5.0 \times 10^{-6}$	-2604.713876	-2604.722436	-2604.706421	-2603.931704	-2603.915245	3515	3612	
TZ	$5.0 \times 10^{-5}$	-2604.882296	-2604.890842	-2604.875037	-2604.101958	-2604.085561	3469	3599	
	$3.0 \times 10^{-5}$	-2604.882276	-2604.890839	-2604.875030	-2604.098312	-2604.082083	3470	3562	
	$1.5 \times 10^{-5}$	-2604.882200	-2604.890781	-2604.874966	-2604.098467	-2604.082223	3471	3565	
	$9.0 \times 10^{-6}$	-2604.882145	-2604.890738	-2604.874917	-2604.098405	-2604.082176	3472	3562	
	$5.0 \times 10^{-6}$	-2604.882107	-2604.890711	-2604.874884	-2604.098630	-2604.082379	3473	3567	
QZ	$5.0 \times 10^{-5}$	-2604.919564	-2604.928141	-2604.912282	-2604.139351	-2604.122914	3481	3608	
	$3.0 \times 10^{-5}$	-2604.919758	-2604.928350	-2604.912491	-2604.136693	-2604.120350	3481	3587	
	$1.5 \times 10^{-5}$	-2604.919916	-2604.928527	-2604.912666	-2604.135511	-2604.119233	3481	3573	
	$9.0 \times 10^{-6}$	-2604.919954	-2604.928581	-2604.912716	-2604.135646	-2604.119338	3482	3579	
	$5.0 \times 10^{-6}$	-2604.919963	-2604.928604	-2604.912734	-2604.136107	-2604.119858	3483	3566	

\* Spin-orbit splitting in  $\text{cm}^{-1}$  (experimental value:<sup>86</sup> 3685  $\text{cm}^{-1}$ ).

Table 3: Wall Times\* ( $T_2$  in seconds) for PT2 Corrections in sf-X2C-iCIPT2, SOiCI, and 4C-iCIPT2 calculations of Br ( $3d^{10}4s^24p^5$ ).

Basis set	$C_{\min}$	sf-X2C-iCIPT2		SOiCI		4C-iCIPT2		4C-iCIPT2 <sup>a</sup>	
		$ P ^{b,c}$	$T_2$	$ P ^{b,d}$	$T_2^e$	$ P ^b$	$T_2^f$	$ P ^b$	$T_2$
DZ	$5.0 \times 10^{-5}$	146949	48.9	297306	139.2 [2.85]	66809	440.6 [3.16]	18148	12.5
	$3.0 \times 10^{-5}$	266972	64.2	541068	167.7 [2.61]	115839	759.6 [4.53]	28080	14.0
	$1.5 \times 10^{-5}$	582319	112.8	1187558	245.7 [2.18]	267706	1716.7 [6.99]	50239	16.8
	$9.0 \times 10^{-6}$	1022725	167.6	2092972	319.0 [1.90]	513195	3314.9 [10.4]	75532	20.6
	$5.0 \times 10^{-6}$	1906432	281.6	3915296	507.4 [1.80]	998099	6386.7 [12.6]	118985	25.5
TZ	$5.0 \times 10^{-5}$	248384	141.6	500826	286.1 [2.02]	115189	1380.7 [4.82]	57106	35.1
	$3.0 \times 10^{-5}$	550019	249.1	1108046	425.7 [1.71]	247380	3999.9 [9.40]	103112	53.4
	$1.5 \times 10^{-5}$	1533813	597.6	3093278	958.8 [1.60]	590573	12678.1 [13.2]	217305	94.8
	$9.0 \times 10^{-6}$	2967699	1040.4	5998268	1737.4 [1.67]	1175598	22453.7 [12.9]	345719	145.5
	$5.0 \times 10^{-6}$	5930752	2047.4	12023362	3286.5 [1.61]	2504958	52175.4 [15.9]	563638	228.0
QZ	$5.0 \times 10^{-5}$	313293	310.3	630388	484.6 [1.56]	155843	3724.6 [7.69]	89896	92.3
	$3.0 \times 10^{-5}$	740258	688.9	1487852	1052.9 [1.53]	332023	10342.9 [9.82]	170270	164.0
	$1.5 \times 10^{-5}$	2222671	1889.9	4470458	2887.8 [1.53]	840020	32005.5 [11.1]	381604	363.3
	$9.0 \times 10^{-6}$	4667946	3897.4	9403060	6063.9 [1.56]	1686352	71487.5 [11.8]	674228	675.5
	$5.0 \times 10^{-6}$	10325265	8535.1	20843428	13209.3 [1.55]	3866697	174537.7 [13.2]	1276668	1199.8

\* Performed on a single node with two Hygon 7285 CPUs (32 cores at 2.0 GHz) and 512 GB DDR4 memory.

<sup>a</sup> Only  $4s^24p^5$  electrons are correlated.

<sup>b</sup> Size of variation space.

<sup>c</sup> Summation of the number of CSFs for each irrep of  $D_{2h}$ .

<sup>d</sup> Summation of the number of CSFs for each irrep of  $D_{2h}$ , weighted by spin multiplicity.

<sup>e</sup> Relative cost with respect to sf-X2C-iCIPT2.

<sup>f</sup> Relative cost with respect to SOiCI.

Table 4: Linear Fits of PT2 Wall Times versus Sizes of Variational Spaces (see Table 3) for sf-X2C-iCIPT2, SOiCI and 4C-iCIPT2 calculations of Br ( $3d^{10}4s^24p^5$ ).

Basis set	sf-X2C-iCIPT2		SOiCI		4C-iCIPT2		4C-iCIPT2 <sup>a</sup>	
	Slope <sup>b</sup>	$R^2$	Slope <sup>b</sup>	$R^2$	Slope <sup>b</sup>	$R^2$	Slope <sup>b</sup>	$R^2$
DZ	1.32	0.9991	1.00	0.998	63.9	0.99998	1.30	0.997
TZ	3.34	0.9997	2.61	0.99989	211	0.998	3.81	0.9989
QZ	8.20	0.99991	6.29	0.9997	445	0.99990	9.38	0.998

<sup>a</sup> Only  $4s^24p^5$  electrons are correlated.

<sup>b</sup> Multiplied by  $10^4$ .

## 5 Conclusion and Outlook

By utilizing advanced C++ features, such as template metaprogramming and polymorphism, a highly modular, extendable, and efficient platform, dubbed MetaWave, has been introduced for unified implementation of many-electron wavefunctions. It is composed of three abstract layers, i.e., infrastructure, Hamiltonian, and wavefunction. The infrastructure layer supplies unified interfaces for basic linear algebra operations and algorithm tem-

plates for parallel computing, abstracting scalar type dependencies and parallel strategies. The Hamiltonian layer addresses domain-specific components such as Hamiltonians, MPBFs, symmetries, integrals, and matrix elements, employing a type-trait and tagging system. The wavefunction layer implements high-level computational algorithms, benefiting from the abstractions provided by the infrastructure and Hamiltonian layers. In this way, Hamiltonians, wavefunctions, and parallel strategies are decoupled to the maximal extent, thereby reducing code repetition and enhancing code extendability for new functionalities. Among others, some immediate developments include (1) GPU acceleration of both matrix-vector products and perturbation corrections, (2) support of more and general Hamiltonians for the extension of MetaWave to a wider range of fermionic and/or bosonic quantum systems, and (3) support of tensor contractions for unified implementation of relativistic and nonrelativistic coupled-cluster methods.

## Notes

The authors declare no competing financial interest.

## Acknowledgments

This work was supported by National Natural Science Foundation of China (Grant No. 22373057) and Mount Tai Scholar Climbing Project of Shandong Province.

## Data availability

All data are available in this article.

## References

- (1) Liu, W. Perspective: Simultaneous treatment of relativity, correlation, and QED. *WIREs Comput. Mol. Sci.* **2023**, *13*, e1652.
- (2) Liu, W.; Lindgren, I. Going beyond “no-pair relativistic quantum chemistry”. *J. Chem. Phys.* **2013**, *139*, 014108.
- (3) Liu, W. Advances in relativistic molecular quantum mechanics. *Phys. Rep.* **2014**, *537*, 59–89.
- (4) Liu, W. Essentials of relativistic quantum chemistry. *J. Chem. Phys.* **2020**, *152*, 180901.
- (5) Liu, W. Comment on “Theoretical examination of QED Hamiltonian in relativistic molecular orbital theory” [J. Chem. Phys. 159, 054105 (2023)]. *J. Chem. Phys.* **2024**, *160*, 187101.
- (6) Liu, W. Unified construction of relativistic Hamiltonians. *J. Chem. Phys.* **2024**, *160*, 084111.
- (7) Zhang, N.; Liu, W. Unified Implementation of Relativistic Wave Function Methods: 4C-iCIPT2 as a Showcase. *J. Chem. Theory Comput.* **2024**, *20*, 9003–9017.
- (8) Schollwöck, U. The density-matrix renormalization group in the age of matrix product states. *Ann. Phys.* **2011**, *326*, 96–192.
- (9) Chan, G. K.-L.; Sharma, S. The density matrix renormalization group in quantum chemistry. *Annu. Rev. Phys. Chem.* **2011**, *62*, 465–481.
- (10) Chan, G. K.-L. Low entanglement wavefunctions. *WIREs: Comput. Mol. Sci.* **2012**, *2*, 907–920.

- (11) Olivares-Amaya, R.; Hu, W.; Nakatani, N.; Sharma, S.; Yang, J.; Chan, G. K.-L. The ab-initio density matrix renormalization group in practice. *J. Chem. Phys.* **2015**, *142*, 034102.
- (12) Wouters, S.; Neck, D. V. The density matrix renormalization group for ab initio quantum chemistry. *Eur. Phys. J. D* **2014**, *68*, 272.
- (13) Szalay, S.; Pfeffer, M.; Murg, V.; Barcza, G.; Verstraete, F.; Schneider, R.; Legeza, Ö. Tensor product methods and entanglement optimization for ab initio quantum chemistry. *Int. J. Quantum Chem.* **2015**, *115*, 1342–1391.
- (14) Baiardi, A.; Reiher, M. The density matrix renormalization group in chemistry and molecular physics: Recent developments and new challenges. *J. Chem. Phys.* **2020**, *152*, 040903.
- (15) Liu, W.; Hoffmann, M. R. iCI: Iterative CI toward full CI. *J. Chem. Theory Comput.* **2016**, *12*, 1169–1178, (E) **2016**, *12*, 3000.
- (16) Zhang, N.; Liu, W.; Hoffmann, M. R. Iterative Configuration Interaction with Selection. *J. Chem. Theory Comput.* **2020**, *16*, 2296–2316.
- (17) Zhang, N.; Liu, W.; Hoffmann, M. R. Further Development of iCIPT2 for Strongly Correlated Electrons. *J. Chem. Theory Comput.* **2021**, *17*, 949–964.
- (18) Guo, Y.; Zhang, N.; Lei, Y.; Liu, W. iCISCF: An Iterative Configuration Interaction-Based Multiconfigurational Self-Consistent Field Theory for Large Active Spaces. *J. Chem. Theory Comput.* **2021**, *17*, 7545–7561.
- (19) Holmes, A. A.; Tubman, N. M.; Umrigar, C. J. Heat-bath configuration interaction: an efficient selected configuration interaction algorithm inspired by heat-bath sampling. *J. Chem. Theory Comput.* **2016**, *12*, 3674–3680.

- (20) Garniron, Y.; Scemama, A.; Loos, P.-F.; Caffarel, M. Hybrid stochastic-deterministic calculation of the second-order perturbative contribution of multireference perturbation theory. *J. Chem. Phys.* **2017**, *147*, 034101.
- (21) Holmes, A. A.; Umrigar, C. J.; Sharma, S. Excited states using semistochastic heat-bath configuration interaction. *J. Chem. Phys.* **2017**, *147*, 164111.
- (22) Sharma, S.; Holmes, A. A.; Jeanmairet, G.; Alavi, A.; Umrigar, C. J. Semistochastic Heat-Bath Configuration Interaction Method: Selected Configuration Interaction with Semistochastic Perturbation Theory. *J. Chem. Theory Comput.* **2017**, *13*, 1595–1604.
- (23) Li, J.; Otten, M.; Holmes, A. A.; Sharma, S.; Umrigar, C. J. Fast semistochastic heat-bath configuration interaction. *J. Chem. Phys.* **2018**, *149*, 214110.
- (24) Smith, J. E. T.; Mussard, B.; Holmes, A. A.; Sharma, S. Cheap and near exact CASSCF with large active spaces. *J. Chem. Theory Comput.* **2017**, *13*, 5468–5478.
- (25) Yao, Y.; Umrigar, C. J. Orbital Optimization in Selected Configuration Interaction Methods. *J. Chem. Theory Comput.* **2021**, *17*, 4183–4194.
- (26) Zhang, T.; Evangelista, F. A. A deterministic projector configuration interaction approach for the ground state of quantum many-body systems. *J. Chem. Theory Comput.* **2016**, *12*, 4326–4337.
- (27) Schriber, J. B.; Evangelista, F. A. Communication: An adaptive configuration interaction approach for strongly correlated electrons with tunable accuracy. *J. Chem. Phys.* **2016**, *144*, 161106.
- (28) Schriber, J. B.; Evangelista, F. A. Adaptive configuration interaction for computing challenging electronic excited states with tunable accuracy. *J. Chem. Theory Comput.* **2017**, *13*, 5354–5366.

- (29) Schriber, J. B.; Hannon, K. P.; Li, C.; Evangelista, F. A. A Combined Selected Configuration Interaction and Many-Body Treatment of Static and Dynamical Correlation in Oligoacenes. *J. Chem. Theory Comput.* **2018**, *14*, 6295–6305.
- (30) Tubman, N. M.; Lee, J.; Takeshita, T. Y.; Head-Gordon, M.; Whaley, K. B. A deterministic alternative to the full configuration interaction quantum Monte Carlo method. *J. Chem. Phys.* **2016**, *145*, 044112.
- (31) Lehtola, S.; Tubman, N. M.; Whaley, K. B.; Head-Gordon, M. Cluster decomposition of full configuration interaction wave functions: A tool for chemical interpretation of systems with strong correlation. *J. Chem. Phys.* **2017**, *147*, 154105.
- (32) Tubman, N. M.; Levine, D. S.; Hait, D.; Head-Gordon, M.; Whaley, K. B. An efficient deterministic perturbation theory for selected configuration interaction methods. **2018**, arXiv preprint arXiv:1808.02049.
- (33) Levine, D. S.; Hait, D.; Tubman, N. M.; Lehtola, S.; Whaley, K. B.; Head-Gordon, M. CASSCF with Extremely Large Active Spaces Using the Adaptive Sampling Configuration Interaction Method. *J. Chem. Theory Comput.* **2020**, *16*, 2340–2354.
- (34) Chilkuri, V. G.; Neese, F. Comparison of many-particle representations for selected-CI I: A tree based approach. *J. Comput. Chem.* **2021**, *42*, 982–1005.
- (35) Chilkuri, V. G.; Neese, F. Comparison of Many-Particle Representations for Selected Configuration Interaction: II. Numerical Benchmark Calculations. *J. Chem. Theory Comput.* **2021**, *17*, 2868–2885.
- (36) Zhang, N.; Xiao, Y.; Liu, W. SOiCI and iCISO: combining iterative configuration interaction with spin-orbit coupling in two ways. *J. Phys.: Condens. Matter* **2022**, *34*, 224007.

- (37) Guo, Y.; Zhang, N.; Liu, W. SOiCISCF: Combining SOiCI and iCISCF for Variational Treatment of Spin–Orbit Coupling. *J. Chem. Theory Comput.* **2023**, *19*, 6668–6685.
- (38) Mussard, B.; Sharma, S. One-Step Treatment of Spin–Orbit Coupling and Electron Correlation in Large Active Spaces. *J. Chem. Theory Comput.* **2017**, *14*, 154–165.
- (39) Wang, X.; Sharma, S. Relativistic Semistochastic Heat-Bath Configuration Interaction. *J. Chem. Theory Comput.* **2023**, *19*, 848–855.
- (40) Sharma, S.; Chan, G. K.-L. Spin-adapted density matrix renormalization group algorithms for quantum chemistry. *J. Chem. Phys.* **2012**, *136*, 124121.
- (41) Keller, S.; Reiher, M. Spin-adapted matrix product states and operators. *J. Chem. Phys.* **2016**, *144*, 134101.
- (42) Battaglia, S.; Keller, S.; Knecht, S. Efficient relativistic density-matrix renormalization group implementation in a matrix-product formulation. *J. Chem. Theory Comput.* **2018**, *14*, 2353–2369.
- (43) Menczer, A.; van Damme, M.; Rask, A.; Huntington, L.; Hammond, J.; Xanthreas, S. S.; Ganahl, M.; Legeza, O. Parallel implementation of the Density Matrix Renormalization Group method achieving a quarter petaFLOPS performance on a single DGX-H100 GPU node. *J. Chem. Theory Comput.* **2024**, *20*, 8397–8404.
- (44) Kriebel, M. H.; Tecmer, P.; Gałyńska, M.; Leszczyk, A.; Boguslawski, K. Accelerating Pythonic Coupled-Cluster Implementations: A Comparison Between CPUs and GPUs. *J. Chem. Theory Comput.* **2024**, *20*, 1130–1142.
- (45) Chan, M.; Verstraelen, T.; Tehrani, A.; Richer, M.; Yang, X. D.; Kim, T. D.; Vöhringer-Martinez, E.; Heidar-Zadeh, F.; Ayers, P. W. The tale of HORTON: Lessons learned in a decade of scientific software development. *J. Chem. Phys.* **2024**, *160*, 162501.

- (46) Kim, T. D.; Richer, M.; Sánchez-Díaz, G.; Miranda-Quintana, R. A.; Verstraelen, T.; Heidar-Zadeh, F.; Ayers, P. W. Fanpy: A python library for prototyping multideterminant methods in ab initio quantum chemistry. *J. Comput. Chem.* **2023**, *44*, 697–709.
- (47) Kim, T. D.; Miranda-Quintana, R. A.; Richer, M.; Ayers, P. W. Flexible ansatz for N-body configuration interaction. *Comput. Theor. Chem.* **2021**, *1202*, 113187.
- (48) Miranda-Quintana, R. A.; Kim, T. D.; Lokhande, R. A.; Richer, M.; Sánchez-Díaz, G.; Gaikwad, P. B.; Ayers, P. W. Flexible Ansatz for N-Body Perturbation Theory. *J. Phys. Chem. A* **2024**, *128*, 3458–3467.
- (49) Epstein, P. S. The stark effect from the point of view of Schroedinger's quantum theory. *Phys. Rev.* **1926**, *28*, 695.
- (50) Nesbet, R. K. Configuration interaction in orbital theories. *Proc. Roy. Soc. London. Ser. A* **1955**, *230*, 312–321.
- (51) Evangelista, F. A.; Li, C.; Verma, P.; Hannon, K. P.; Schriber, J. B.; Zhang, T.; Cai, C.; Wang, S.; He, N.; Stair, N. H.; et al. Forte: A Suite of Advanced Multireference Quantum Chemistry Methods. **2024**, arXiv preprint arXiv:2405.10197.
- (52) Shao, Y.; Gan, Z.; Epifanovsky, E.; Gilbert, A. T.; Wormit, M.; Kussmann, J.; Lange, A. W.; Behn, A.; Deng, J.; Feng, X.; et al. Advances in molecular quantum chemistry contained in the Q-Chem 4 program package. *Mol. Phys.* **2015**, *113*, 184–215.
- (53) Neese, F. Software update: The ORCA program system—Version 5.0. *WIREs Comput. Mol. Sci.* **2022**, *12*, e1606.
- (54) Garniron, Y.; Applencourt, T.; Gasperich, K.; Benali, A.; Ferté, A.; Paquier, J.; Pradines, B.; Assaraf, R.; Reinhardt, P.; Toulouse, J.; et al. Quantum Package 2.0: An

- Open-Source Determinant-Driven Suite of Programs. *J. Chem. Theory Comput.* **2019**, *15*, 3591–3609.
- (55) Sharma, S. Dice. <https://github.com/sanshar/Dice>, last accessed on 03/19/25.
- (56) Zhang, Y.; Suo, B.; Wang, Z.; Zhang, N.; Li, Z.; Lei, Y.; Zou, W.; Gao, J.; Peng, D.; Pu, Z.; et al. BDF: A relativistic electronic structure program package. *J. Chem. Phys.* **2020**, *152*, 064113.
- (57) Peng, D.; Ma, J.; Liu, W. On the construction of Kramers paired double group symmetry functions. *Int. J. Quantum Chem.* **2009**, *109*, 2149–2167.
- (58) Paldus, J.; Boyle, M. J. Unitary group approach to the many-electron correlation problem via graphical methods of spin algebras. *Phys. Script.* **1980**, *21*, 295–311.
- (59) Shavitt, I. Graph theoretical concepts for the unitary group approach to the many-electron correlation problem. *Int. J. Quantum Chem. (Symp.)* **1977**, *11*, 131–149.
- (60) Chan, G. K.-L.; Keselman, A.; Nakatani, N.; Li, Z.; White, S. R. Matrix product operators, matrix product states, and ab initio density matrix renormalization group algorithms. *J. Chem. Phys.* **2016**, *145*, 014102.
- (61) Brorsen, K. R. Quantifying Multireference Character in Multicomponent Systems with Heat-Bath Configuration Interaction. *J. Chem. Theory Comput.* **2020**, *16*, 2379–2388.
- (62) Alaal, N.; Brorsen, K. R. Multicomponent heat-bath configuration interaction with the perturbative correction for the calculation of protonic excited states. *J. Chem. Phys.* **2021**, *155*, 234107.
- (63) Haugland, T. S.; Ronca, E.; Kjørstad, E. F.; Rubio, A.; Koch, H. Coupled Cluster Theory for Molecular Polaritons: Changing Ground and Excited States. *Phys. Rev. X* **2020**, *10*, 041043.

- (64) Matoušek, M.; Vu, N.; Govind, N.; Foley IV, J. J.; Veis, L. Polaritonic chemistry using the density matrix renormalization group method. *J. Chem. Theory Comput.* **2024**, *20*, 9424–9434.
- (65) Castagnola, M.; Riso, R. R.; Barlini, A.; Ronca, E.; Koch, H. Polaritonic response theory for exact and approximate wave functions. *WIREs Comput. Mol. Sci.* **2024**, *14*, e1684.
- (66) Buenker, R. J.; Peyerimhoff, S. D. Individualized configuration selection in CI calculations with subsequent energy extrapolation. *Theor. Chem. Acta* **1974**, *35*, 33–58.
- (67) Huron, B.; Malrieu, J. P.; Rancurel, P. Iterative perturbation calculations of ground and excited state energies from multiconfigurational zeroth-order wave functions. *J. Chem. Phys.* **1973**, *58*, 5745–5759.
- (68) Giner, E.; Scemama, A.; Caffarel, M. Using perturbatively selected configuration interaction in quantum Monte Carlo calculations. *Can. J. Chem.* **2013**, *91*, 879–885.
- (69) Angeli, C.; Cimiraglia, R.; Persico, M.; Toniolo, A. Multireference perturbation CI I. Extrapolation procedures with CAS or selected zero-order spaces. *Theor. Chem. Acc.* **1997**, *98*, 57–63.
- (70) Huang, C.; Liu, W.; Xiao, Y.; Hoffmann, M. R. iVI: An iterative vector interaction method for large eigenvalue problems. *J. Comput. Chem.* **2017**, *38*, 2481–2499, (E) **2018**, *39*, 338.
- (71) Huang, C.; Liu, W. iVI-TD-DFT: An iterative vector interaction method for exterior/interior roots of TD-DFT. *J. Comput. Chem.* **2019**, *40*, 1023–1037, (E) **2018**, *39*, 338.
- (72) USCiLab cereal. <https://github.com/USCiLab/cereal>, last accessed on 03/19/25.
- (73) Li, Z.; Xiao, Y.; Liu, W. On the spin separation of algebraic two-component relativistic Hamiltonians. *J. Chem. Phys.* **2012**, *137*, 154114.

- (74) Li, Z.; Xiao, Y.; Liu, W. On the spin separation of algebraic two-component relativistic Hamiltonians: Molecular properties. *J. Chem. Phys.* **2014**, *141*, 054111.
- (75) Kutzelnigg, W.; Liu, W. Quasirelativistic theory equivalent to fully relativistic theory. *J. Chem. Phys.* **2005**, *123*, 241102.
- (76) Liu, W.; Peng, D. Exact two-component Hamiltonians revisited. *J. Chem. Phys.* **2009**, *131*, 031104.
- (77) Balabanov, N. B.; Peterson, K. A. Systematically convergent basis sets for transition metals. I. All-electron correlation consistent basis sets for the 3d elements Sc–Zn. *J. Chem. Phys.* **2005**, *123*, 064107.
- (78) Boguslawski, K.; Leszczyk, A.; Nowak, A.; Brzęk, F.; Żuchowski, P. S.; Kędziera, D.; Tecmer, P. Pythonic Black-box Electronic Structure Tool (PyBEST). An open-source Python platform for electronic structure calculations at the interface between chemistry and physics. *Comput. Phys. Commun.* **2021**, *264*, 107933.
- (79) Boguslawski, K.; Brzęk, F.; Chakraborty, R.; Cieślak, K.; Jahani, S.; Leszczyk, A.; Nowak, A.; Sujkowski, E.; Świerczyński, J.; Ahmadkhani, S.; et al. PyBEST: Improved functionality and enhanced performance. *Comput. Phys. Commun.* **2024**, *297*, 109049.
- (80) Saue, T.; Bast, R.; Gomes, A. S. P.; Jensen, H. J. A.; Visscher, L.; Aucar, I. A.; Di Remigio, R.; Dylla, K. G.; Eliav, E.; Fasshauer, E.; et al. The DIRAC code for relativistic molecular calculations. *J. Chem. Phys.* **2020**, *152*, 204104.
- (81) Eriksen, J. J.; Anderson, T. A.; Deustua, J. E.; Ghanem, K.; Hait, D.; Hoffmann, M. R.; Lee, S.; Levine, D. S.; Magoulas, I.; Shen, J.; et al. The Ground State Electronic Energy of Benzene. *J. Phys. Chem. Lett.* **2020**, *11*, 8922–8929.
- (82) Song, Y.; Guo, Y.; Lei, Y.; Zhang, N.; Liu, W. The Static–Dynamic–Static Family of

- Methods for Strongly Correlated Electrons: Methodology and Benchmarking. *Top. Current Chem.* **2021**, 379, 1–56.
- (83) Song, Y.; Zhang, N.; Lei, Y.; Guo, Y.; Liu, W. QUEST#4X: An Extension of QUEST#4 for Benchmarking Multireference Wave Function Methods. *J. Chem. Theory Comput.* **2025**, 21, 1119–1135.
- (84) Wilson, A. K.; Woon, D. E.; Peterson, K. A.; Dunning, J., Thom H. Gaussian basis sets for use in correlated molecular calculations. IX. The atoms gallium through krypton. *J. Chem. Phys.* **1999**, 110, 7667–7676.
- (85) de Jong, W. A.; Harrison, R. J.; Dixon, D. A. Parallel Douglas–Kroll energy and gradients in NWChem: Estimating scalar relativistic effects using Douglas–Kroll contracted basis sets. *J. Chem. Phys.* **2001**, 114, 48–53.
- (86) Kramida, A.; Ralchenko, Y.; Reader, J.; Team, N. A. S. D. NIST Atomic Spectra Database, version 5.12. <http://physics.nist.gov/asd>, last accessed on 03/19/25.

TOC graphic

